Mathematically similar movement kernels yield contrasting ecological outcomes in insect trapping

Danish A. Ahmed

Department of Mathematics and Natural Sciences, Gulf University for Science and Technology, Hawally, Kuwait

*Corresponding author (Ahmed.D@gust.edu.kw)

Abstract

Insect movement is often described using random-walk models but comparing ecological outcomes of short- and long-distance movement can depend on how their underlying movement kernels are related. Here, thin- and heavy-tailed step-length distributions are linked through a common survival probability and then optimally compared using a similarity measure, providing an objective comparison when an independent ecological basis is lacking. Because the optimal relationship differs among spatial dimensions, we examine its consequences across three insect-trapping systems: one-dimensional trap cropping, where pests are attracted from a cash crop to a terminal trap crop and may be retained, removed or emigrate; two-dimensional pitfall trapping, where randomly moving ground-dwelling arthropods encounter passive traps; and three-dimensional flight interception, where flying insects may encounter, be captured by, or bypass a finite panel. Across these systems, optimally related movement kernels produced contrasting ecological outcomes. In trap-cropping, the relative advantage of long-distance movement depended on attraction strength and trap-crop allocation, reversing from greater to lower removal as attraction increased. In pitfall trapping, long-distance movement generally increased cumulative capture within a confined spatial domain, with trap counts increasing with survival probability. However, non-optimal values could produce similar capture to short-distance movement, potentially masking the effect of movement type. In the flight interception model, long-distance movement reduced panel interception and capture while increasing edge leakage. Thus, mathematically optimal similarity between movement kernels does not ensure ecological equivalence. Rather, the remaining differences in displacement structure interact with behavioural responses, boundary effects and trapping geometry, producing outcomes that vary among ecological contexts.

Keywords Insect movement, Random walks, Movement kernels, Trap cropping, Pitfall trapping, Flight interception, Planar trapping

1. Introduction

Insect movement is a fundamental driver of ecological dynamics, linking individual behaviour to processes ranging from resource acquisition and habitat use to population redistribution, biological invasions, disease transmission and species interactions (Turchin 1998; Bullock et al. 2002; Bowler and Benton 2005; Nathan et al. 2008; Hooten et al. 2017). Random-walk models provide a widely used framework for describing such movement at the

individual level, representing trajectories as sequences of discrete displacements whose statistical properties determine how rapidly individuals explore space (Kareiva and Shigesada 1983; Berg 1993; Codling et al. 2008). In movement ecology, the probability distribution describing spatial displacement over a given time interval is commonly represented as a movement kernel, providing a mechanistic link between individual trajectories and population-level spatial redistribution. A particularly important distinction is between short-distance, scale-specific movement and long-distance, scale-free movement. Brownian-type random walks are characterised by thin-tailed step-length distributions with finite variance, whereas Lévy-type movement is associated with a heavy-tail in which occasional very long movements occur more frequently (Viswanathan et al. 2000; Benhamou 2007; James et al. 2011; Reynolds 2018). Both forms of movement have been used extensively in ecological theory and empirical interpretation, with Brownian-like behaviour often associated with local movement or resource-rich environments (Kareiva 1983), whereas Lévy-like behaviour has been proposed under conditions involving long relocations or spatially extensive search (Bartumeus et al. 2005; Benhamou 2007; Reynolds et al. 2013). These differences extend beyond the appearance of individual trajectories: the tail structure of the underlying movement kernel can influence rates of spatial spread, boundary crossing, encounters with ecological targets and other emergent population-level outcomes (Kot 2001; Petrovskii et al. 2014; Bearup et al. 2016; Ellis et al. 2019).

A key question, however, is determining how short- and long-distance movement processes should be compared (Kawai and Petrovskii 2012). For thin-tailed movement kernels, movement scales can often be related through finite moments such as the mean-squared displacement, allowing random-walk processes to be compared on the basis of equivalent spatial spread, but such moment-based comparisons are not generally applicable to heavy-tailed movement because the step-length variance may be infinite (Codling et al. 2008). Previous theoretical studies have instead related Brownian- and Lévy-type movement by requiring the same tail survival probability p of executing a displacement longer than a characteristic distance l_c. Yet the value of p may be experiment-specific or lack a general criterion, with potentially important consequences for ecological outcomes (Rodrigues et al. 2015; Bearup et al. 2016; Choules and Petrovskii 2017; Ellis et al. 2019). An objective relationship can be obtained by imposing a common survival probability, $P(l > l_c) = p$, and identifying an optimal value p^* that minimises the squared Euclidean distance between the step-length distributions (Ahmed et al. 2025). This is particularly useful when no independent ecological basis exists for choosing p. However, mathematically relating two movement kernels does not imply that they are ecologically interchangeable. Even at the optimal relationship, the distributions retain fundamentally different shapes, particularly in their tails, and repeated movement can amplify relatively modest differences at the step level into pronounced differences in spatial redistribution and encounter processes (Ahmed et al. 2025). This raises a broader ecological question: whether mathematically similar short- and long-distance movement processes produce comparable ecological outcomes, particularly when encounters with spatial targets or boundaries are influenced by long steps and spatial geometry (Petrovskii et al. 2014; Ahmed and Petrovskii 2019; Ahmed et al. 2023).

Insect interception and trapping provide a useful set of systems in which to investigate these ecological consequences because capture is intrinsically movement-dependent: an individual must first reach, cross or intersect a target before it can be retained or removed (Miller et al. 2015). The geometry of these encounters changes naturally across spatial dimensions. Trap cropping, in which an attractive crop diverts pests away from a cash crop, can be conceptualised in one-dimensional space as movement along a linear agricultural landscape towards a terminal trap-crop strip (Ahmed et al. 2026b), with the diamondback moth (*Plutella xylostella*) as a well-studied example (Badenes-Perez et al. 2004). Effective control depends not only on attraction, but also on pest redistribution, interception, retention and mortality after arrival (Hokkanen 1991; Shelton and Badenes-Pérez 2006; Cook et al. 2007; Holden 2026a). Movement behaviour is therefore central to whether insects reach and remain within the interception zone or subsequently emigrate. In two dimensions, passive pitfall trapping offers a complementary ecological setting in which variation in the movement behaviour of ground-dwelling arthropods, such as ground beetles (*Poecilus cupreus*), affects trap encounters (Bailey et al. 2021). Pitfall captures are influenced by several factors, including movement activity, trap number, trap size and inter-trap spacing, as well as spatial configuration (Brown and Matthews 2016; Hohbein and Conway 2018; Ahmed and Petrovskii 2019; Ahmed et al. 2023). Consequently, pitfall catches reflect an activity–density relationship, where capture depends not only on the abundance of individuals but also on their movement activity (Thomas et al. 1998). Typical sampling strategies, such as grid and transect spatial arrangements, provide contrasting geometries for examining how spatial arrangement influences movement-dependent capture (Crist and Wiens 1995; Larsen and Forsyth 2005). For flying insects, movement and trap encounters naturally extend into three-dimensional space, with species such as mosquitoes (*Aedes aegypti*; *Anopheles gambiae*) and fruit flies (*Drosophila melanogaster*) providing relevant examples for flight tracking and interception studies (Butail et al. 2012; Vaxenburg et al. 2025; Jimenez-Vallejo et al. 2026; Le Roy et al. 2026). Three-dimensional random-walk models have also been used to represent movement incorporating directional bias, persistence and spatial exploration (Ahmed et al. 2021b; Klappstein et al. 2026). Finite planar surfaces such as sticky panels and coloured cards are commonly used for monitoring flying insects (Epsky et al. 2008; Benthall et al. 2022). Under directional bias towards the target, short- and long-distance trajectories can interact differently with finite trap geometry through patterns of panel interception, repeated contact and edge crossing, with consequences for captures.

Here, we examine the ecological consequences of linking short- and long-distance movement kernels within three insect-trapping systems: trap cropping of insect pests, pitfall trapping of ground-dwelling arthropods, and planar interception of flying insects. Our aim is to determine how mathematical similarity between the movement kernels translates into ecological outcomes such as interception, capture and removal once movement interacts with habitat boundaries, trap configurations and surfaces, and whether the resulting differences are consistent or context-dependent across spatial dimensions.

2. One-dimensional random walk movement and trap cropping

2.1 Linking Gaussian and Cauchy displacements

The one-dimensional case represents movement along a single spatial axis. If an individual is located at x_{i-1}, its position after movement step i is

$$x_i = x_{i-1} + \Delta x_i, \quad (1)$$

where Δx_i is the signed displacement during the i^{th} step. For Brownian movement, increments are sampled from a zero-centred Gaussian distribution, $\Delta x_i \sim \mathcal{N}(0, \sigma^2)$, where σ defines the characteristic movement scale over one movement interval Δt. The corresponding probability density is

$$\phi_{\mathrm{G}}(\Delta x|\sigma) = \frac{1}{\sigma\sqrt{2\pi}} \exp\left(-\frac{\Delta x^2}{2\sigma^2}\right). \quad (2)$$

Lévy-type movement is represented by a Cauchy distribution,

$$\phi_{\mathrm{C}}(\Delta x|\gamma) = \frac{\gamma}{\pi(\gamma^2+\Delta x^2)}, \quad (3)$$

where γ is the Cauchy scale parameter. These movement kernels differ by the rate of decay in the tails: the Gaussian distribution is thin-tailed, has finite variance and characterises short-distance movement, whereas the Cauchy distribution is heavy-tailed, has infinite variance and characterises long-distance movement.

The two distributions can be related by requiring the same tail probability p of executing a step exceeding a characteristic step length l_c, i.e., $P(|\Delta x| > l_c) = p$. For the Gaussian and Cauchy distributions, respectively,

$$l_c = \sigma\sqrt{2}\mathrm{erfc}^{-1}(p), \quad l_c = \gamma \tan\left[\frac{\pi}{2}(1-p)\right]. \quad (4)$$

Equating the corresponding characteristic step lengths l_c gives the following relationship between the movement scales:

$$\frac{\gamma}{\sigma} = \frac{\sqrt{2}\mathrm{erfc}^{-1}(p)}{\tan\left[\frac{\pi}{2}(1-p)\right]}. \quad (5)$$

expressed solely as a function of p. To obtain an objective relationship, the squared Euclidean distance between the Gaussian and Cauchy probability densities

$$d(\phi_{\mathrm{C}}, \phi_{\mathrm{G}}) = \int_{-\infty}^{\infty} [\phi_{\mathrm{C}}(\Delta x|\gamma) - \phi_{\mathrm{G}}(\Delta x|\sigma)]^2 d\Delta x, \quad (6)$$

is minimised, which occurs at $p^* = 0.721$, $\frac{\gamma}{\sigma} = 0.762$, and characteristic step length $l_c^* = 0.357\sigma$ (Ahmed et al. 2025). This defines the optimal similarity relationship between the movement kernels in one-dimensional space.

2.2 Trap cropping of insect pests

We represent a trap-cropping system as a one-dimensional field of total length L, partitioned into a cash crop occupying $0 \leq x \leq kL$ and a trap crop occupying $kL < x \leq L$, where $0 <$

$k < 1$ is the proportion of the field allocated to the cash crop. This formulation allows land allocation to be considered alongside attraction and retention, which are important components of trap-cropping performance (Holden 2026b). A population of N_0 insects is initially distributed uniformly throughout the cash crop. Movement is simulated in discrete time steps of Δt over a total duration T. At movement step i, position is updated according to

$$x_i = x_{i-1} + \delta_i l_i, \tag{7}$$

where δ_i denotes movement direction, taking the value -1 for movement away from the trap crop and $+1$ for movement towards it, and $l_i = |\Delta x_i|$ is the step length during the i^{th} movement step. Individuals may move beyond either field boundary, to $x < 0$ or $x > L$, where they are classified as emigrated while outside the field but remain active and may subsequently re-enter. Within the cash crop, short- and long-distance movement are generated from the magnitudes of the Gaussian and Cauchy displacement distributions in Eqs. (2) and (3), respectively, and are linked through the tail survival probability, with $p^* = 0.721$ defining the optimal one-dimensional relationship.

Movement direction within the cash crop is biased towards the trap crop according to

$$\beta(x) = \beta_{\max} \cdot \frac{x}{kL}, \tag{8}$$

where $\beta_{\max}$ determines the maximum attraction strength at the cash crop–trap crop interface, with attraction increasing linearly with x. This bias may arise from orientation towards trap-crop-associated cues, including host-plant volatiles and aggregation pheromones that can direct pest movement towards attractive plants (Landolt et al. 1999; Martel et al. 2005; Brzozowski et al. 2020). The probabilities of moving towards $(+)$ and away $(-)$ from the trap crop are therefore

$$P(\delta_i = \pm 1) = \frac{1 \pm \beta(x)}{2}. \tag{9}$$

Following entry into the trap crop, both types of movement switch to unbiased Gaussian movement, with behavioural arrestment represented by a reduction in movement scale,

$$\sigma_{\text{trap}} = \rho\sigma, \tag{10}$$

where $0 < \rho \leq 1$ determines the strength of arrestment, with smaller values indicating stronger local confinement and longer residence within the trap crop. Such arrestment may arise when insects settle on a preferred host and shift towards more localised movement associated with feeding or host exploitation (Badenes-Pérez et al. 2005; Gui et al. 2012; Boiteau et al. 2014). Outside the field, individuals are unaffected by trap-crop attraction, as the associated directional cues are assumed not to extend beyond the cropped area, or by arrestment, which is associated with residence within the trap crop. They therefore resume their respective Gaussian or Cauchy movement process at the full scale.

Two removal processes operate following trap-crop encounter. On entry, an insect is removed with probability α_{entry}, representing interception at the cash crop–trap crop boundary, such as contact with an insecticide-treated border or sticky trap plants, physical trapping, or edge-focused predation (Holden et al. 2012; Macfadyen and Muller 2013). The limiting case $\alpha_{\text{entry}} = 1$ represents perfect entry interception and an idealised dead-end trap-crop scenario (Badenes-Pérez 2025). Those that survive entry are subsequently exposed to a daily removal probability α_{day} while resident within the trap crop, representing mortality or other removal processes acting during residence. This is converted to the corresponding per-step probability according to

$$\alpha_{\text{step}} = 1 - \left(1 - \alpha_{\text{day}}\right)^{\Delta t/24}, \tag{11}$$

where Δt is measured in hours. The entry-triggered process is applied on each crossing from the cash crop into the trap crop, including subsequent re-entry, whereas within-trap removal operates only during residence within the trap crop. Removal is an absorbing outcome, while surviving insects may move between the cash crop, trap crop and emigration states. Rare long-distance steps that traverse the entire trap-crop strip are still treated as trap-crop encounters.

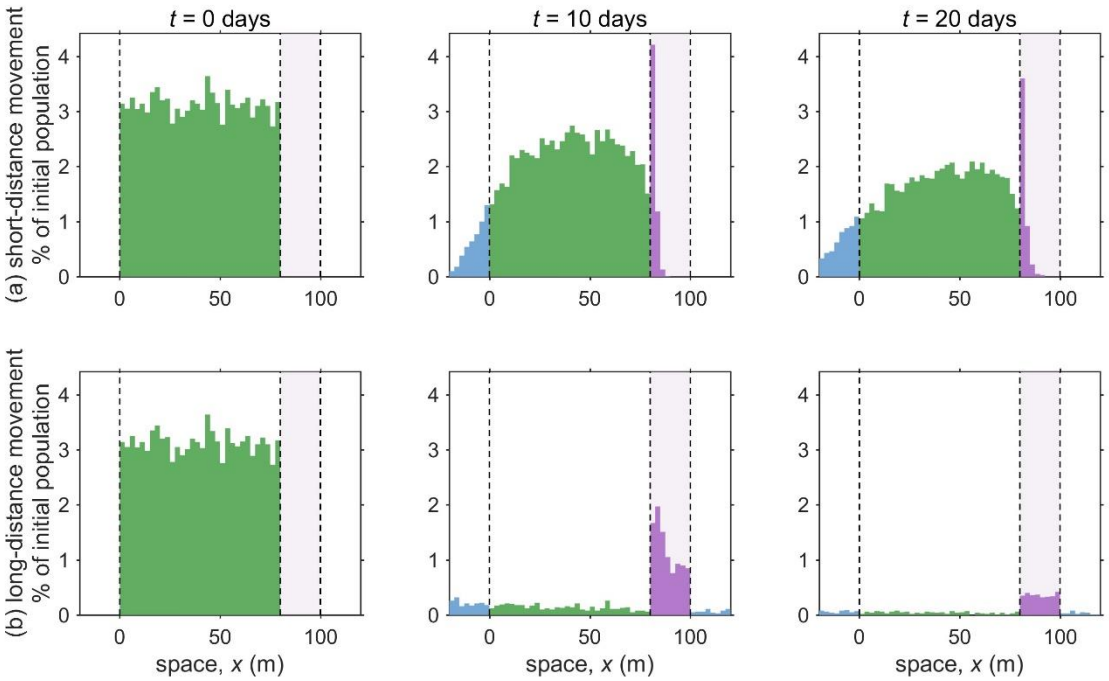


Figure 1 Trap cropping dynamics in one-dimensional space. Histograms with 2.5 m spatial bins show insect population (%) at $t = 0$, 10 and 20 days for (a) short-distance Gaussian movement and (b) optimally linked long-distance Cauchy movement. The field has total length $L = 100$ m, with an 80 m cash crop and a 20 m trap crop ($k = 0.8$). $N_0 = 10^4$ individuals are initially distributed uniformly within the cash crop. Movement occurs in discrete time steps of $\Delta t = 0.5$ h. Short-distance movement uses Gaussian displacements with scale $\sigma = 0.5$ m, whereas long-distance movement uses Cauchy displacements with scale γ determined from the optimal relationship $p^* = 0.721$, giving $\gamma = 0.381$ m. Within the cash crop, movement is biased towards the trap crop through a linear attraction profile with maximum strength $\beta_{\max} = 0.1$. Following entry into the trap crop, both movement types switch to unbiased Gaussian movement with $\rho = 1/3$, giving a reduced scale $\sigma_{\text{trap}} = 0.167$ m

and representing behavioural arrestment. Entry-triggered removal occurs with probability $\alpha_{\text{entry}} = 0.1$, while removal during trap-crop residence occurs with daily probability $\alpha_{\text{day}} = 0.2$. Green, purple and blue histogram bars represent the population (%) located in the cash crop, trap crop and emigration zones, respectively; the shaded purple region denotes the trap crop.

Under short-distance movement (Figure 1a), individuals remained broadly distributed across the cash crop, although occupancy gradually declined over time. Within the trap crop, individuals became concentrated near the cash crop–trap crop interface, while emigration occurred only through the left field boundary. Under long-distance movement (Figure 1b), cash-crop occupancy declined more rapidly, leaving few individuals within the cash crop by day 10 and about 1% remaining by day 20. A concentration also developed near the cash crop–trap crop interface but extended further into the trap crop. Emigration occurred across both field boundaries at similar levels.

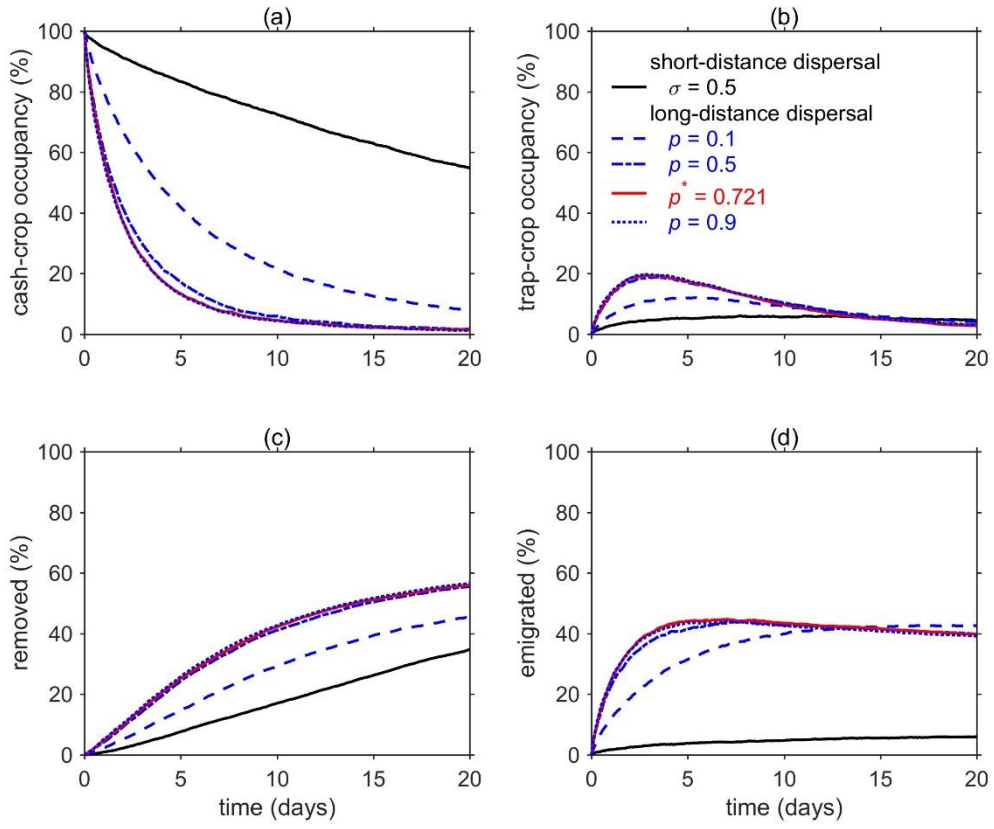


Figure 2 Trap-cropping dynamics under short- and long-distance movement. Temporal evolution over 20 days of (a) cash-crop occupancy, (b) trap-crop occupancy, (c) cumulative removal and (d) emigration beyond either field boundary. All quantities are expressed as % of the initial population, $N_0 = 10^4$; the four states are mutually exclusive and sum to 100% at each time point. Short-distance movement is represented by Gaussian movement with $\sigma = 0.5$ m (black). Long-distance Cauchy movement is shown for $p = 0.1$, 0.5 and 0.9 (blue), corresponding to $\gamma = 0.130$, 0.337 and 0.397 m, respectively, together with the optimally related case $p^* = 0.721$ ($\gamma = 0.381$ m; red). All other model parameters are as in Figure 1.

Cash-crop occupancy declined under all movement cases, reaching about 55% of the initial population after 20 days under short-distance movement and only 1–8% under long-distance movement (Figure 2a). Trap crop occupancy peaked at about 6% under short-distance

movement and at about 12–20% under long-distance movement, with the long-distance peaks occurring earlier before declining towards similar levels by day 20 (Figure 2b). Cumulative removal reached about 34% under short-distance movement and 45–55% under long-distance movement (Figure 2c), while emigration remained low under short-distance movement but reached around 40% under the long-distance cases by day 20 (Figure 2d). Among the long-distance cases, $p = 0.1$ showed a slower decline in cash-crop occupancy, a lower trap-crop peak and lower cumulative removal than the higher-p cases, whereas $p = 0.5$, the optimal case $p^* = 0.721$, and $p = 0.9$ produced closely similar dynamics.

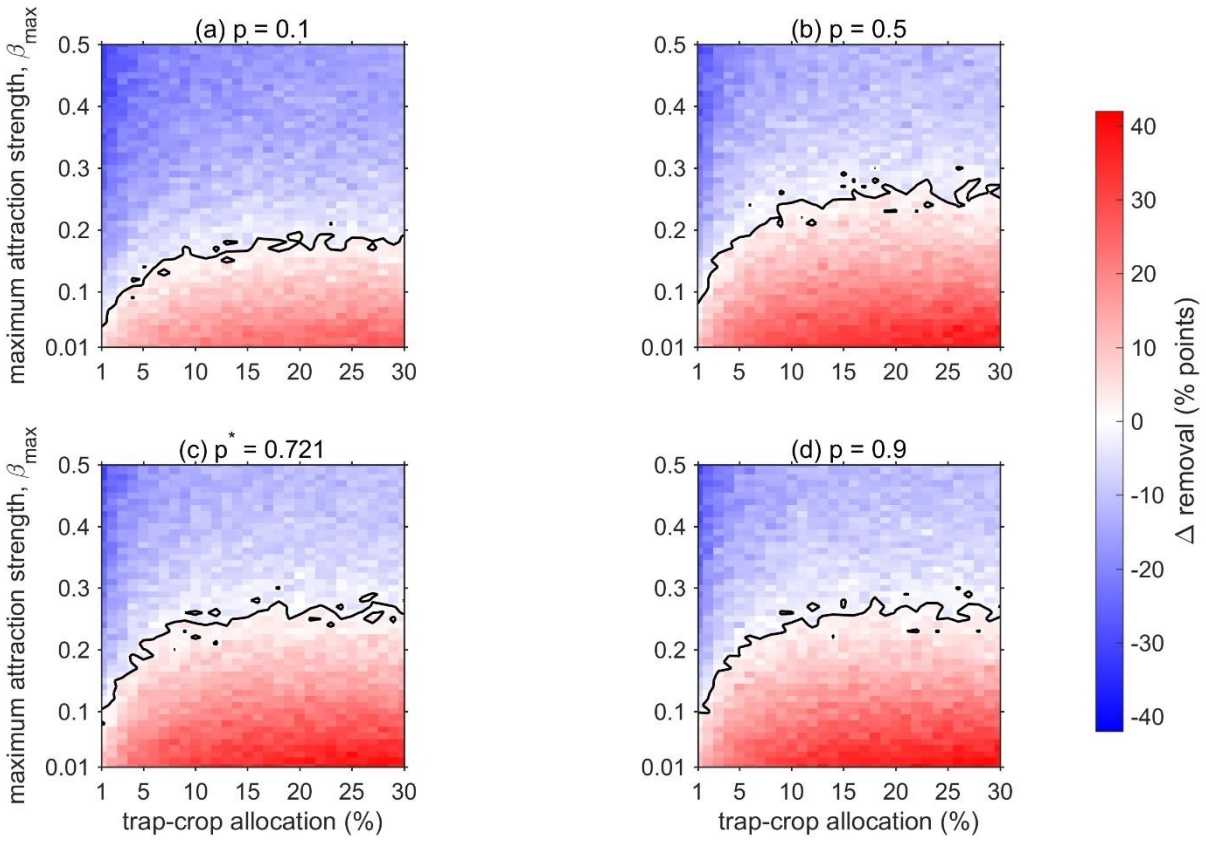


Figure 3 Heat maps showing the %-point difference in cumulative removal between long- and short-distance movement (Δ removal) after 20 days, across trap-crop allocation and attraction strength, $\beta_{\max}$. Δ removal > 0 indicates greater removal under long-distance movement (red), Δ removal < 0 indicates greater removal under short-distance movement (blue), and Δ removal ≈ 0 indicates similar removal under the two movement processes (white). The solid black contour denotes Δ removal = 0 and marks the transition between parameter combinations producing greater removal under long- or short-distance movement. Trap-crop allocation, $1 - k$, was varied from 1% to 30% of the field, while maximum attraction strength, $\beta_{\max}$, was varied from 0.01 to 0.50. Panels show the long-distance cases (a) $p = 0.1$, (b) $p = 0.5$, (c) the optimally related case $p^* = 0.721$, and (d) $p = 0.9$. Simulations used $N_0 = 10^3$ individuals for each parameter combination; all other model parameters are as in Figure 1.

Figure 3 showed that the effect of movement type on cumulative removal depended strongly on attraction strength. At low $\beta_{\max}$, long-distance movement produced greater removal than short-distance movement across most trap-crop allocations, with differences reaching about 30–40 %-points in parts of the parameter space. As $\beta_{\max}$ increased, this difference

diminished and then reversed. For $p = 0.1$, similar removal for both movement processes generally occurred around $\beta_{\max} \approx 0.1$–0.2 once trap-crop allocation exceeded about 10% (Figure 3a). For $p \geq 0.5$, including the optimal case $p^* = 0.721$, this transition occurred at higher attraction strengths, generally around $\beta_{\max} \approx 0.2$–0.3 as trap-crop allocation increased (Figure 3b–d). Thus, all long-distance cases showed the same reversal from greater removal under long-distance movement at weaker attraction to greater removal under short-distance movement at stronger attraction. Trap-crop allocation affected the transition most when less than ≈ 10% of the field was allocated to the trap crop. Beyond this allocation, the transition boundary remained relatively stable despite further increases in trap-crop area. As a result, attraction strength was the main determinant of which movement process produced greater removal, while trap-crop allocation primarily modified the position of this transition at low allocation.

3. Two-dimensional random walk movement and pitfall trapping

3.1 Linking Rayleigh and folded-Cauchy step lengths

In two-dimensional space, an individual movement path is represented as a sequence of discrete steps linking successive locations. If the individual is at position $\mathbf{x}_{i-1} = (x_{i-1}, y_{i-1})$, its position after the i^{th} movement step is

$$\mathbf{x}_i = \mathbf{x}_{i-1} + \Delta\mathbf{x}_i, \tag{12}$$

where $\Delta\mathbf{x}_i = (\Delta x_i, \Delta y_i)$ is the displacement vector over one movement interval Δt. Each displacement is characterised by a step length $l_i = |\mathbf{x}_i - \mathbf{x}_{i-1}|$ and orientation θ_i, such that $\Delta x_i = l_i \cos(\theta_i)$ and $\Delta y_i = l_i \sin(\theta_i)$. For the unbiased and uncorrelated movement considered here, successive orientations are independent and uniformly distributed over $(-\pi, \pi]$, so that there is no directional persistence.

With independent Gaussian displacement components, $\Delta x_i, \Delta y_i \sim \mathcal{N}(0, \sigma^2)$, the resulting step length follows a Rayleigh distribution,

$$\phi_{\mathrm{R}}(l|\sigma) = \frac{l}{\sigma^2} \exp\left(-\frac{l^2}{2\sigma^2}\right), \tag{13}$$

This distribution is thin-tailed, with mean step length and variance

$$E[l] = \sigma\frac{\sqrt{2\pi}}{2}, \ \ \mathrm{Var}(l) = (4-\pi)\frac{\sigma^2}{2}. \tag{14}$$

Lévy-type movement is represented by a folded-Cauchy step-length distribution,

$$\phi_{\mathrm{fC}}(l|\gamma) = \frac{2\gamma}{\pi(\gamma^2 + l^2)}, \tag{15}$$

where γ is the corresponding scale parameter. The folded-Cauchy distribution is heavy-tailed, with $\phi_{fC}(l) \sim l^{-2}$as $l \to \infty$, and has neither a finite mean nor variance.

For a common survival probability p, the characteristic step lengths for the Rayleigh and folded-Cauchy distributions are, respectively,

$$l_c = \sigma\sqrt{-2\ln p}, \qquad l_c = \gamma \tan\left[\frac{\pi}{2}(1-p)\right]. \tag{16}$$

Equating these characteristic step lengths gives the relationship

$$\frac{\gamma}{\sigma} = \frac{\sqrt{-2\ln p}}{\tan\left[\frac{\pi}{2}(1-p)\right]}. \tag{17}$$

The corresponding squared Euclidean distance between the Rayleigh and folded-Cauchy step-length distributions is

$$d(\phi_{\mathrm{fC}}, \phi_{\mathrm{R}}) = \int_0^\infty [\phi_{\mathrm{fC}}(l|\gamma) - \phi_{\mathrm{R}}(l|\sigma)]^2 dl, \tag{18}$$

with $\frac{\gamma}{\sigma}$ expressed as a function of p through the survival-probability relationship. Minimising this distance gives $p^* = 0.658$, $\frac{\gamma}{\sigma} = 1.536$, with corresponding characteristic step length $l_c^* = 0.915\sigma$ (Ahmed et al. 2025).

3.2 Pitfall trapping of ground-dwelling arthropods

The movement of ground-dwelling arthropods was simulated within a two-dimensional circular sampling domain of radius R. Nine identical circular pitfall traps, each with radius r, were placed in two spatial arrangements. In the grid configuration, traps formed a 3×3 regular array centred on the origin, while in the transect configuration, nine traps were positioned along the horizontal axis with equal spacing. These arrangements were chosen to represent two commonly used pitfall-sampling configurations while maintaining the same number and size of traps. Empirical pitfall-trapping studies vary widely in spatial scale and design, but community monitoring often uses around 8–12 traps over relatively small sampling areas, with trap radii of about 0.05 m (Work et al. 2002; Brown and Matthews 2016), while commonly used inter-trap spacings are around 5–10 m (Ward et al. 2001; Hohbein and Conway 2018).

At the start of each simulation, individuals were distributed independently and uniformly across the circular domain. To ensure uniform sampling by area, the angular coordinate was drawn as $\theta \sim \mathrm{Unif}(0, 2\pi)$, while $U \sim \mathrm{Unif}(0, 1)$, giving the initial position $\mathbf{x}_0 = R\sqrt{U}(\cos\theta\,, \sin\theta)$. Those individuals initially located within any trap were removed prior to the first movement step. The remaining individuals defined the effective initial population N_0 separately for the grid and transect configurations, and all subsequent capture proportions were calculated relative to this post-exclusion population. This follows the virtual-trapping framework in which randomly distributed individuals move independently through a landscape containing fixed passive traps and are removed following trap encounters (Ahmed et al. 2023).

Short-distance movement was represented by a two-dimensional Gaussian random walk with Rayleigh-distributed step lengths (Eq. 13), with mean step length given by Eq.

(14). To provide an ecologically interpretable movement scale, the mean ground movement speed was set to $v = 2.5$ mh^{-1}, based on empirical estimates for actively moving carabid beetles such as *Pterostichus melanarius* (Wallin and Ekbom 1988). With movement simulated at fixed time intervals of $\Delta t = 10$ min and $E[l] = v\Delta t$, this gives a mean step length of $E[l] = 0.417$ m and $\sigma = 0.332$ m. Long-distance movement was represented by Lévy-type movement with folded-Cauchy step lengths (Eq. 15). The scale parameter γ was related to σ through the common survival probability p using Eq. (17), with the optimal relationship occurring at $p^* = 0.658$.

Individuals were confined to the circular sampling domain throughout the simulations. At each movement step, a candidate endpoint was generated from the corresponding movement distribution. If the endpoint fell outside the domain, the movement was rejected and redrawn until the resulting position satisfied $|\mathbf{x}| \leq R$. The same boundary procedure was applied to both short- and long-distance movement. Because the random-walk model is formulated as a position-jump process, trap interception may occur between successive recorded positions, particularly during long steps. Each movement segment was therefore sampled at S equally spaced intermediate locations,

$$x_{i,s} = x_{i-1} + \frac{s}{S}\Delta x_i, \quad s = 1, \ldots, S. \tag{19}$$

At each sampled location, the distance to every trap centre was calculated. An individual was captured if any sampled location fell inside a trap, after which it was removed from the population. This sub-step procedure improves the detection of trap interceptions between successive recorded positions (Ahmed et al. 2021a).

Cumulative trap capture at time t was calculated from the number of individuals remaining in the sampling domain, $N(t)$, relative to the effective initial population N_0,

$$C(t) = 100\left[1 - \frac{N(t)}{N_0}\right]. \tag{20}$$

This measure was used to compare capture dynamics across movement processes and trap configurations.

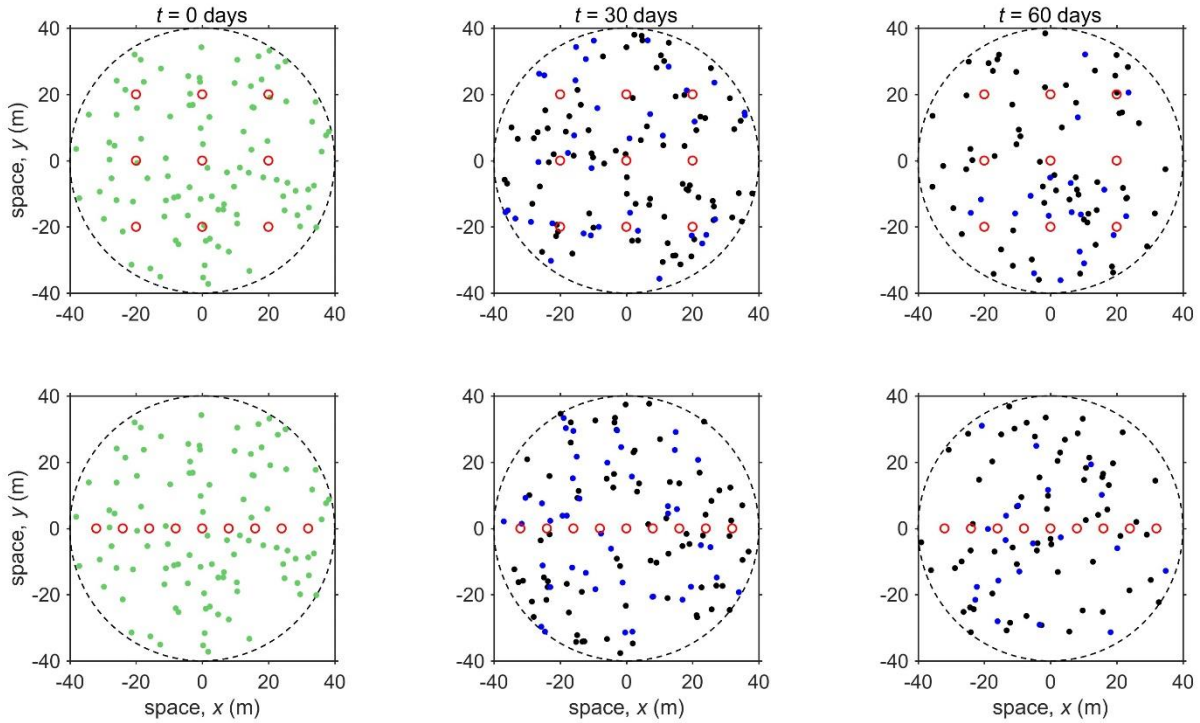


Figure 4 Pitfall trapping under short- and long-distance movement within a circular sampling domain of radius $R = 40$ m (0.5 ha; dashed circle). Nine circular pitfall traps (red circles), each of radius $r = 0.05$ m, were arranged either as a 3×3 regular grid with 20 m inter-trap spacing (top row) or along a linear transect with 8 m inter-trap spacing (bottom row). A total of 100 individuals were initially distributed uniformly within the domain, with the same initial spatial realisation used for both trap configurations and movement processes. In this realisation, no individuals were initially located within a trap, so the effective initial population was $N_0 = 100$ for both configurations. Columns show population distributions at $t = 0$, 30 and 60 days. Green points denote initial positions, while black and blue points denote surviving individuals under short- and long-distance movement, respectively. Short-distance movement used $\sigma = 0.332$ m, corresponding to a mean ground movement speed of 2.5 mh^{-1} and movement interval $\Delta t = 10$ min. Long-distance movement used folded-Cauchy step lengths for the optimally related case $p^* = 0.658$, with $\gamma = 0.511$ m. Each movement segment was sampled at $S = 100$ intermediate locations to detect trap interceptions.

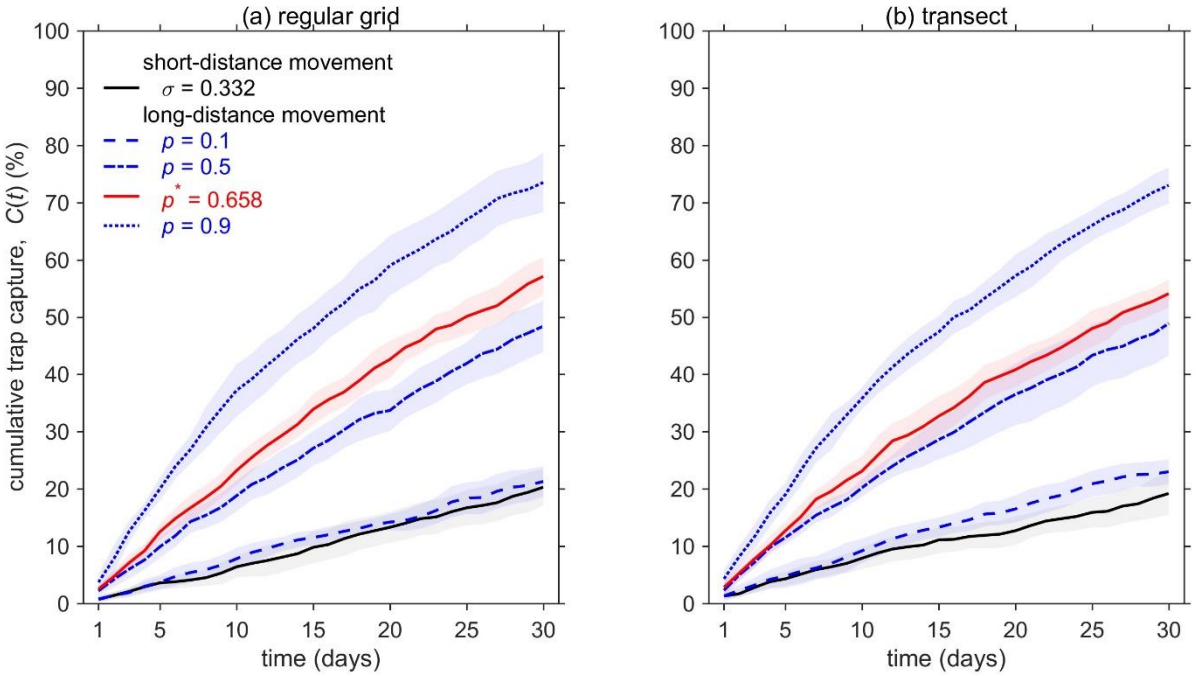


Figure 5 Cumulative trap capture, $C(t)$, over 30 days under short- and long-distance movement for (a) the regular 3 × 3 grid and (b) the linear transect configurations. Each simulation run began with $N_0 = 10^2$ individuals distributed uniformly across the sampling domain, and cumulative capture was averaged over 10 realisations. The same initial positions were used for the grid and transect before applying trap-specific exclusions; none occurred in any realisation, so $N_0 = 10^2$ throughout. Movement trajectories were then generated independently for each movement case: short-distance movement used $\sigma = 0.332$ m, and long-distance movement used folded-Cauchy step lengths for $p = 0.1$, 0.5, and 0.9, with $\gamma = 0.113$, 0.391, and 0.964 m, respectively. The optimally related case was $p^* = 0.658$, corresponding to $\gamma = 0.511$ m. Shaded regions denote pointwise 95% confidence intervals for the mean cumulative capture across realisations. All other modelling procedures are as in Figure 4.

The spatial snapshots showed that surviving individuals remained broadly distributed across the sampling domain under both movement processes and trap arrangements, with no clear aggregation around individual traps or the field boundary (Figure 4). In contrast, cumulative capture was movement-dependent (Figure 5). After 30 days, short-distance movement produced about 20% capture, whereas long-distance movement increased progressively with p, reaching about 22% at $p = 0.1$, 49% at $p = 0.5$, 56% for the optimally related case $p^* = 0.658$, and 73% at $p = 0.9$. The grid and transect configurations produced broadly similar responses, indicating that movement process had a much greater effect on capture than trap arrangement. Notably, the non-optimal case $p = 0.1$ produced capture trajectories close to those of short-distance movement, with overlapping confidence regions over much of the simulation duration. Based on trap counts alone, these two movement processes could therefore appear to have similar capture efficiency, even though this similarity depends on the relationship between their underlying step-length distributions. Under the optimal relationship $p^* = 0.658$, long-distance movement produced nearly three times the cumulative capture of short-distance movement by day 30. Thus, the choice of p can determine whether movement-related effects on trapping are revealed or obscured; conversely, similar capture rates do not necessarily imply similar underlying movement processes.

4. Three-dimensional random walk movement and flight interception

4.1 Linking Chi and folded-Cauchy step lengths

In three-dimensional space, the same discrete-step framework is extended by adding a vertical coordinate, such that the position after the i^{th} movement step is represented by $\mathbf{x}_i = (x_i, y_i, z_i)$. Each displacement is described by a step length l_i, an azimuthal angle θ_i, and a polar angle φ_i, which together specify the direction of movement in spherical coordinates (Ahmed et al. 2021b; Klappstein et al. 2026). The azimuthal angle specifies direction in the horizontal plane, whereas the polar angle is measured from the vertical axis. For isotropic movement, directions are uniformly distributed over the surface of the unit sphere, such that all orientations are equally probable.

With independent Gaussian displacement components, $\Delta x_i, \Delta y_i, \Delta z_i \sim \mathcal{N}(0, \sigma^2)$, the resulting step length follows a Maxwell distribution, equivalently a Chi distribution with three degrees of freedom (Ahmed et al. 2021b),

$$\phi_\chi(l \mid \sigma) = \frac{2l^2}{\sigma^3\sqrt{2\pi}} \exp\left(-\frac{l^2}{2\sigma^2}\right). \tag{21}$$

This distribution is thin-tailed, with mean step length and variance

$$E[l] = \frac{4\sigma}{\sqrt{2\pi}}, \quad \mathrm{Var}(l) = \left(3 - \frac{8}{\pi}\right)\sigma^2. \tag{22}$$

Lévy-type movement is represented by a folded-Cauchy step-length distribution

$$\phi_{\mathrm{fC}}(l|\gamma) = \frac{2\gamma}{\pi(\gamma^2 + l^2)}. \tag{23}$$

For a common survival probability p, the Chi distribution with three degrees of freedom satisfies

$$P(l > l_c) = Q\left(\frac{3}{2}, \frac{l_c^2}{2\sigma^2}\right) = p, \tag{24}$$

where Q is the regularised upper incomplete gamma function. Hence, the characteristic step lengths for the Chi and folded-Cauchy distributions (Eq. 16) are, respectively,

$$l_c = \sigma\sqrt{2Q^{-1}\left(\frac{3}{2}, p\right)}, \qquad l_c = \gamma \tan\left[\frac{\pi}{2}(1-p)\right] \tag{25}$$

where Q^{-1} denotes the inverse of Q, with respect to its second argument. Equating these characteristic step lengths gives

$$\frac{\gamma}{\sigma} = \frac{\sqrt{2Q^{-1}\left(\frac{3}{2}, p\right)}}{\tan\left[\frac{\pi}{2}(1-p)\right]}. \tag{26}$$

The squared Euclidean distance between the Chi and folded-Cauchy step-length distributions is

$$d(\phi_{\mathrm{fC}}, \phi_{\chi}) = \int_0^{\infty} \left[\phi_{\mathrm{fC}}(l \mid \gamma) - \phi_{\chi}(l \mid \sigma)\right]^2 \, dl, \tag{27}$$

with $\frac{\gamma}{\sigma}$ expressed as a function of p through the survival-probability relationship. Minimising this distance gives $p^* = 0.650$ and $\frac{\gamma}{\sigma} = 2.089$, with corresponding characteristic step length $l_c^* = 1.282\sigma$ (Ahmed et al. 2025).

4.2 Flight interception

To examine interception outcomes under optimally related short- and long-distance movement processes, we simulated individual flight towards a finite planar trapping surface as a discrete-time stochastic process in Cartesian space (Ahmed et al. 2026a). The position of an individual after movement step i was updated according to

$$\mathbf{x}_i = \mathbf{x}_{i-1} + l_i \mathbf{u}_i, \tag{28}$$

where l_i is the step length and $\mathbf{u}_i$ is a unit vector defining the movement direction. Short-distance movement used Chi-distributed step lengths (Eq. 21), while long-distance movement used folded-Cauchy step lengths (Eq. 23) with the optimal relationship $p^*$and corresponding scale parameter relationship obtained from the matching procedure in Eqs. (24–27). Spatial quantities were expressed in centimetres and time in seconds. A movement interval of $\Delta t = 0.02$ s was set to provide sufficient temporal resolution for resolving trajectory intersections with the finite trapping surface (Ings and Chittka 2008), while a nominal mean short-distance flight speed of 25 cms^{-1} was used. This gives $E[l] = 0.5$ cm and therefore $\sigma = 0.313$ cm. These temporal and spatial scales are not intended to represent a specific species, but are consistent with reported flight speeds of relatively small insects under odour and heat cues, including whiteflies (*Bemisia tabaci*) and mosquitoes (*Anopheles gambiae*) (Isaacs et al. 1999; Spitzen et al. 2013). The nominal flight speed was used only to calibrate the short-distance movement scale and does not represent a mean speed for the folded-Cauchy process, whose theoretical mean step length is unbounded.

The trapping surface was represented by a square panel of side length $L = 10$ cm, centred at the origin in the plane $x = 0$. Sticky-card traps used for insect monitoring vary in size and shape, but commonly include panels with dimensions on the order of approximately 10–20 cm per side (Pobozniak et al. 2020). N individuals were released from the plane $x = -d$, with starting positions sampled uniformly within a circular release region of radius R on this plane. A uniform radial position was generated using $U \sim \mathrm{Unif}(0, 1)$, together with an angular position in the release plane $\psi \sim \mathrm{Unif}(0, 2\pi)$, giving

$$\mathbf{x}_0 = (-d, R\sqrt{U}\cos\psi\,, R\sqrt{U}\sin\psi). \tag{29}$$

This sampling procedure represented natural variation in short-range flight approaches to the trapping surface, allowing individuals to arrive from different lateral positions and approach angles rather than following a single release trajectory.

Each individual was assigned a fixed target point on the square panel, $\mathbf{q} = (0, y_{\mathrm{tar}}, z_{\mathrm{tar}})$, where target locations were sampled uniformly across the panel surface, with $y_{\mathrm{tar}} \sim \mathrm{Unif}\left(-\frac{L}{2}, \frac{L}{2}\right)$ and $z_{\mathrm{tar}} \sim \mathrm{Unif}\left(-\frac{L}{2}, \frac{L}{2}\right)$. Before the panel plane was crossed, the preferred direction at movement step i was defined as

$$\mathbf{g}_i = \frac{\mathbf{q}-\mathbf{x}_{i-1}}{\|\mathbf{q}-\mathbf{x}_{i-1}\|}, \tag{30}$$

and movement directions were sampled from a three-dimensional von Mises–Fisher distribution centred on $\mathbf{g}_i$, by $\mathbf{u}_i \sim \mathrm{vMF}(\mathbf{g}_i, \kappa)$. The concentration parameter κ controls the strength of orientation towards the assigned target. When $\kappa = 0$, movement directions are isotropic, whereas increasing values produce progressively stronger bias towards the panel. The same target-oriented mechanism was applied to both movement processes, with no localised directional persistence, such that previous headings did not influence subsequent directions. Following the first crossing of the plane $x = 0$, including crossings outside the finite panel boundaries, this panel-oriented bias was removed, and subsequent headings were sampled uniformly over the unit sphere.

Each trajectory was simulated for a maximum of $n_{\max}$ movement updates, corresponding to a duration of T s, and was terminated earlier if $\|\mathbf{x}\| > 1$ m. These limits prevented exceptionally long displacements from producing computationally unbounded trajectories while keeping the simulations focused on short-range flight dynamics. Panel interception was determined from the full straight-line segment connecting successive positions rather than from endpoint locations alone. This approach is important for long-distance movement steps, which may cross the panel plane even when neither endpoint lies on the finite trapping surface. For a segment connecting positions $\mathbf{x}_i$ and $\mathbf{x}_{i+1}$, a crossing of the plane $x = 0$ was identified when the segment intersected the plane. The fractional distance along the segment to the intersection was then calculated as

$$\tau = -\frac{x_i}{x_{i+1}-x_i}. \tag{31}$$

where $0 \leq \tau \leq 1$. The corresponding intersection point was then

$$\mathbf{x}_{\mathrm{int}} = \mathbf{x}_i + \tau(\mathbf{x}_{i+1} - \mathbf{x}_i). \tag{32}$$

An encounter with the panel occurred when $|y_{\mathrm{int}}| \leq \frac{L}{2}$ and $|z_{\mathrm{int}}| \leq \frac{L}{2}$; crossings outside these limits were treated as passage through the panel plane without interception. Following contact, capture occurred with probability p_{stick}, representing imperfect adhesion or post-contact escape in sticky-trap systems (Benthall et al. 2022; Rehling et al. 2025; Roberts et al. 2025). If capture failed, movement resumed from the intersection point after sampling a post-contact heading from a von Mises–Fisher distribution centred on the outward panel normal $(-1, 0, 0)$, with concentration κ_{post}, restricted to directions with negative x-components. A

small displacement $\epsilon \ll 1$ cm was applied to prevent numerical re-contact, after which step lengths were sampled from the same Chi or folded-Cauchy step length distribution as before contact. The panel-oriented directional bias was not reinstated following this interaction, but subsequent intersections with the panel were treated as additional contact events and subjected to the same capture probability.

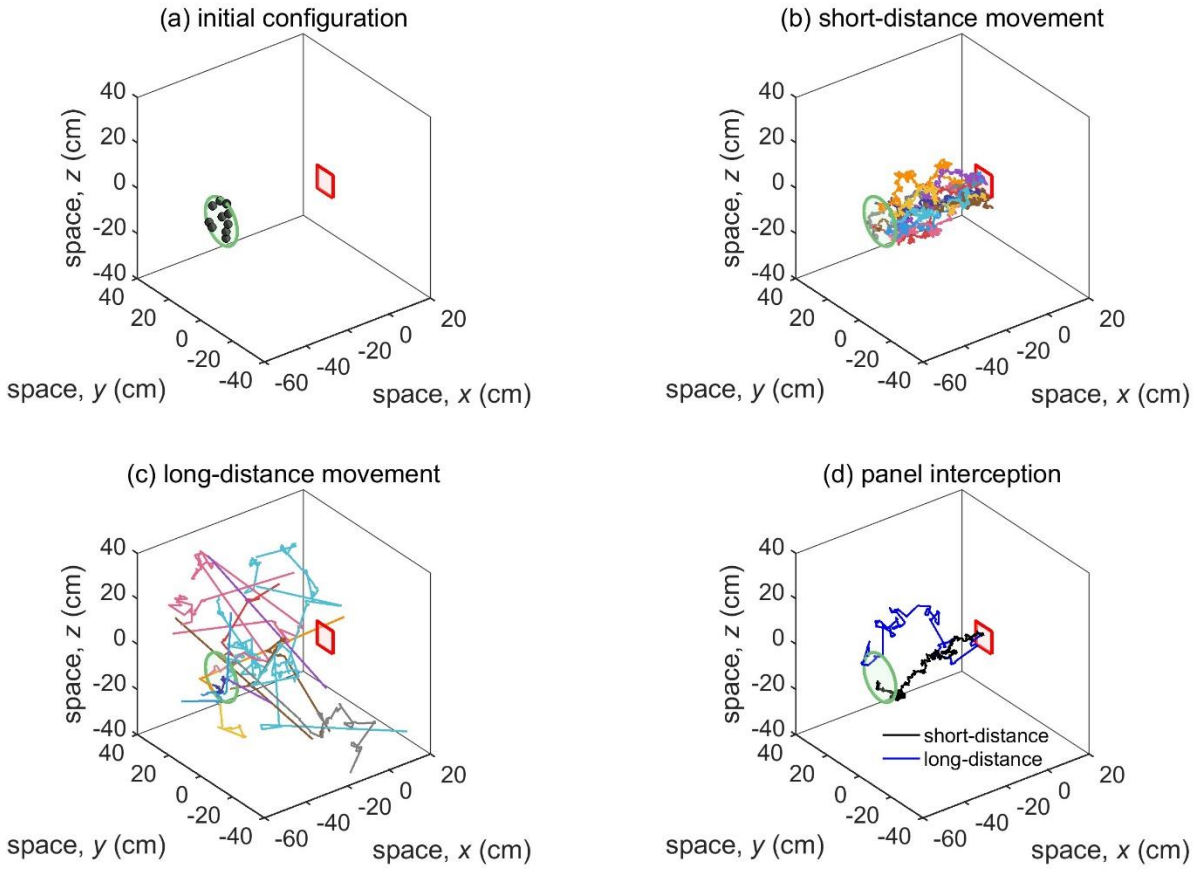


Figure 6 Three-dimensional illustration of the short- and long-distance flight interception framework. (a) Initial configuration showing $N = 10$ individuals with release positions sampled within a circular region of radius $R = 10$ cm on the plane $x = -d = -50$ cm, with the square interception panel of side length $L = 10$ cm centred at the origin on $x = 0$. Realisations generated under (b) short-distance movement, with Maxwell distributed (Chi with three degrees of freedom) step lengths from three-dimensional Gaussian movement ($\sigma = 0.313$ cm), and (c) the optimally related long-distance process, with folded-Cauchy step lengths ($\gamma = 0.655$ cm; $p^* = 0.650$, $\gamma/\sigma = 2.089$). In both cases, movement directions were sampled from a von Mises–Fisher distribution centred on randomly selected target points on the panel surface, with the same concentration parameter $\kappa = 0.3$, and no localised directional persistence. Target-oriented bias was removed after the first crossing of the panel plane. (d) Representative trajectories resulting in panel interception under short-distance Gaussian movement (black) and long-distance folded-Cauchy movement (blue), obtained from the full panel-contact simulations. Trajectories were simulated with $\Delta t = 0.02$s for a maximum of $n_{\max} = 1000$ movement updates, corresponding to a maximum duration of $T = n_{\max}\Delta t = 20$ s. Following unsuccessful panel contact, post-contact movement was implemented with concentration $\kappa_{\text{post}} = 5$ and displacement $\epsilon = 10^{-3}$ cm.

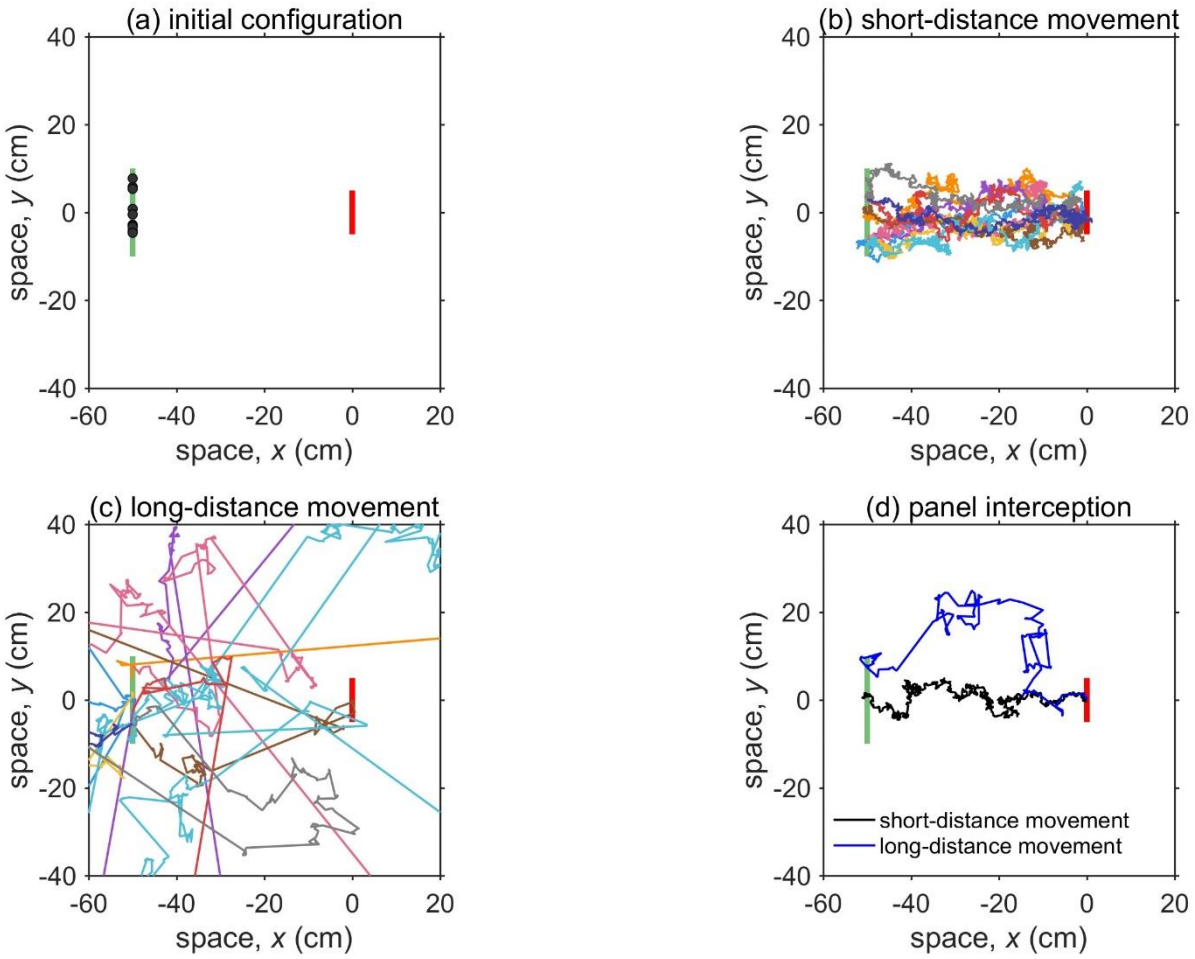


Figure 7 Two-dimensional projection of the three-dimensional flight trajectories shown in Figure 6 onto the x–y plane. Panels (a) show the same trajectory realisations, illustrating the initial configuration, (b) short-distance Gaussian movement, (c) optimally related long-distance folded-Cauchy movement, and (d) representative trajectories resulting in panel interception. The release region is shown as a vertical green line at $x = -50$cm, and the interception panel is shown as a vertical red line at $x = 0$.

Using the optimally related movement scales as a common comparison framework, short-distance Gaussian and long-distance folded-Cauchy movement produced distinctly different realised flight trajectories (Figures 6 and 7). Under the same panel-oriented bias, short-distance trajectories remained relatively concentrated within the release-to-panel corridor, whereas long-distance trajectories showed greater spatial and lateral displacement associated with occasional large steps (Figures 6b,c and 7b,c). Despite these differences in trajectory structure, both movement processes generated trajectories that reached the finite interception panel through different movement paths (Figures 6d and 7d). These contrasting movement patterns provide a mechanistic basis for differences in panel interception and capture outcomes between the two movement processes.

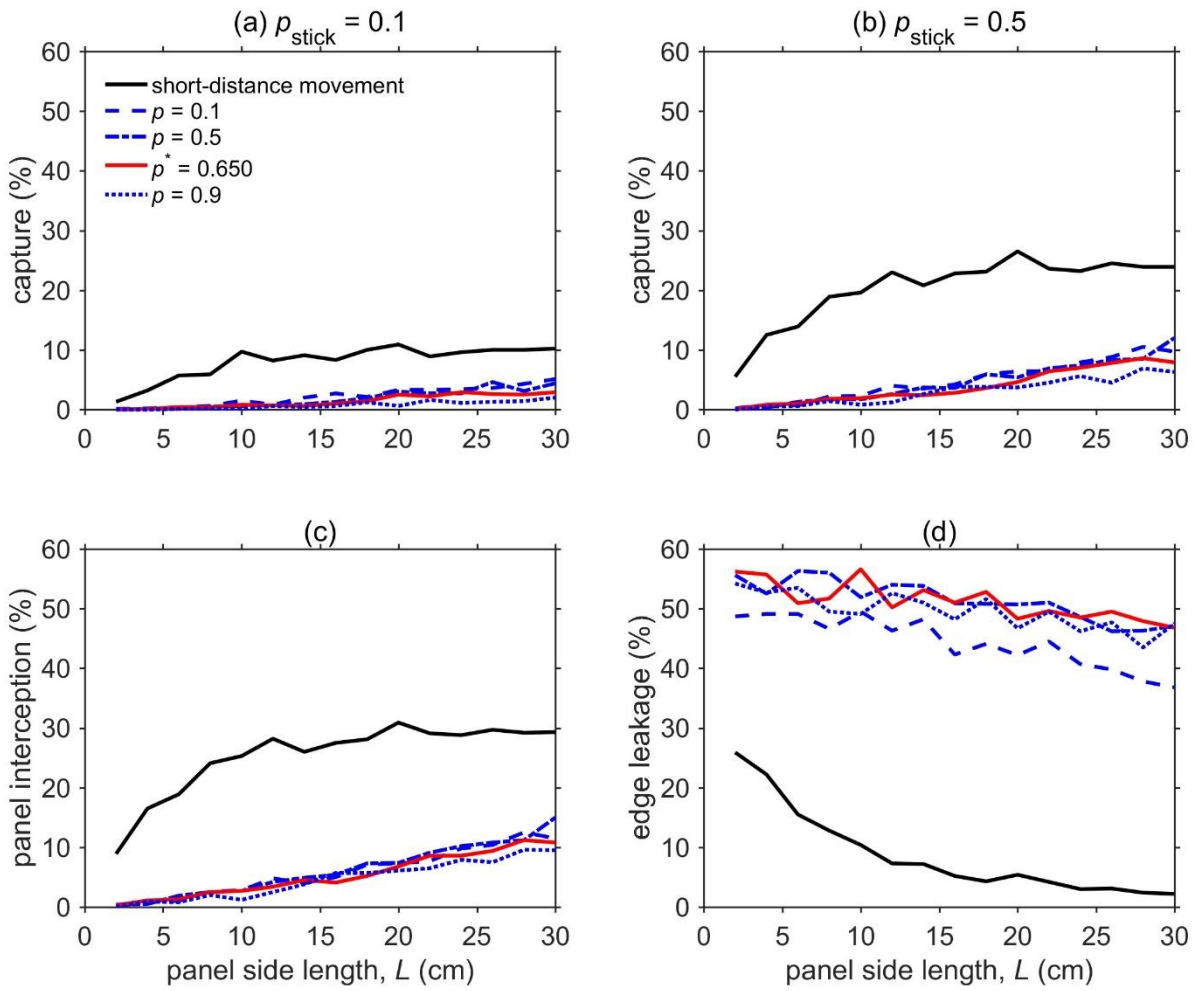


Figure 8 Effects of finite panel size on interception outcomes under short- and long-distance flight movement. Panel side length, L, was varied from 2 to 30 cm for a square panel centred at $x = 0$. Panels show capture (%) following panel contact for (a) $p_{\text{stick}} = 0.1$ and (b) $p_{\text{stick}} = 0.5$. (c) Panel interception (%), defined as the proportion of trajectories crossing the panel plane within the finite panel boundaries, corresponding to the limiting case of $p_{\text{stick}} = 1$, where all panel contacts result in capture. (d) Edge leakage (%), defined as the proportion of trajectories crossing the panel plane outside the finite panel boundaries before any previous panel contact. Short-distance movement was represented by three-dimensional Gaussian movement with Maxwell-distributed (Chi with three degrees of freedom) step lengths (black), whereas long-distance movement was represented by folded-Cauchy step lengths for $p = 0.1$, 0.5 and 0.9 (blue), with the optimally related case $p^* = 0.650$ (red). All other movement, geometric and simulation settings were as in Figure 6. Values were estimated from $N = 1000$ independently simulated trajectories for each panel size and movement process.

Short- and long-distance movement produced contrasting flight interception outcomes when interacting with a finite planar surface (Figure 8). Panel interception (%) increased with panel size under all movement processes, but the magnitude of this increase differed between movement types (Figure 8c). Short-distance Gaussian movement produced consistently higher panel interception, increasing rapidly with panel size before approaching a plateau at larger surfaces. In contrast, folded-Cauchy movement resulted in lower panel interception across the full range of panel sizes, with all long-distance cases remaining within a similar range. The optimally related case, $p^* = 0.650$, produced interception levels similar to the other folded-Cauchy cases and remained distinct from the short-distance Gaussian response.

Capture (%) followed the same general pattern (Figure 8a, b). Increasing panel size improved capture for all movement processes, but short-distance movement consistently resulted in greater capture than long-distance movement. Differences among the folded-Cauchy cases were comparatively small, including the optimally related case, indicating that variation in the long-distance kernel relationship had a weaker influence on capture than the fundamental difference between thin- and heavy-tailed displacement structures. Because capture occurred following panel contact with fixed probabilities $p_{\text{stick}} = 0.1$ and 0.5, these differences primarily reflected variation in panel interception rather than differences in the post-contact capture process.

The contrasting panel interception responses were explained by differences in edge leakage (Figure 8d). Under short-distance Gaussian movement, edge leakage declined as panel size increased, becoming negligible for larger interception surfaces. In comparison, folded-Cauchy movement maintained substantially higher edge-leakage values across all panel sizes, declining only modestly as the panel expanded. Thus, long-distance movement did not simply increase or decrease interception efficiency; rather, heavy-tailed step lengths altered how trajectories interacted with finite geometry by increasing the likelihood of crossing the interception plane outside the panel boundaries. Even when the Gaussian and folded-Cauchy distributions were optimally related, these geometric effects persisted, showing that objectively relating the movement kernels does not remove ecologically important differences in finite interception systems.

5. Discussion

5.1 From movement kernels to ecological outcomes

The relationship between short- and long-distance movement processes has important implications for understanding how dispersal translates into ecological outcomes. Previous theoretical comparisons between thin- and heavy-tailed movement distributions have focused primarily on identifying meaningful relationships between the underlying kernels, particularly because conventional moment-based approaches cannot generally be applied to heavy-tailed processes (Rodrigues et al. 2015; Bearup et al. 2016; Choules and Petrovskii 2017; Ellis et al. 2019). Relating movement distributions through a common survival probability provides an objective framework for comparing short- and long-distance movement when no independent ecological criterion exists for selecting a characteristic scale (Ahmed et al. 2025). However, objectively relating movement distributions does not imply that the ecological processes generated by those movements will be comparable. Even when thin- and heavy-tailed movement kernels are optimally related, they retain different displacement structures, particularly in the frequency of long steps, and these differences can become amplified through repeated movement and interactions with spatial structure. Therefore, the ecological consequences of movement emerge from the interaction between displacement structure and spatial context, rather than from kernel properties alone. Similar amplification of differences between movement processes has been observed in population spread, boundary crossing and spatial redistribution, where rare long-distance events can disproportionately influence ecological dynamics (Petrovskii et al. 2012, 2014; Ellis et al.

2019; Ahmed and Petrovskii 2019; Ahmed et al. 2025). By extending these concepts to contrasting ecological contexts, the present framework highlights that movement kernel comparisons should consider the ecological process being modelled. For mathematical ecologists, this emphasises the importance of coupling dispersal kernels with explicit spatial mechanisms. For applied ecologists, it demonstrates that movement processes can interact with ecological context to produce different ecological outcomes.

5.2 Movement, interception and retention in trap-cropping systems

Trap cropping depends on a sequence of ecological processes: pests must first be attracted towards and encounter the trap crop and then remain there long enough for removal or mortality to occur. Attraction alone is therefore not sufficient for effective suppression, because insects may leave the trap crop or pass through it too quickly for management processes to act (Hokkanen 1991; Shelton and Badenes-Pérez 2006; Cook et al. 2007; Holden et al. 2012; Badenes-Pérez 2025). Previous modelling has similarly shown that trap-crop performance depends on the combined effects of pest movement, attraction, spatial configuration, retention and removal rather than on any single process (Banks and Ekbom 1999; Hannunen 2005; Holden et al. 2012; Fenoglio et al. 2017; Banks and Laubmeier 2024; Holden 2026a, b; Ahmed et al. 2026b). The one-dimensional framework used here builds on this movement-based representation, in which attraction promotes movement towards the trap crop, behavioural arrestment increases residence following entry, and removal can occur either upon entry or during residence within the trap crop (Ahmed et al. 2026b). Our results show that trap-cropping outcomes also depend on how frequently pests make long movements. Under weak attraction, long-distance movement generally produced greater cumulative removal than short-distance movement, because occasional large displacements increased the likelihood of pests reaching and entering the trap crop. As attraction increased, however, this advantage weakened and eventually reversed, with short-distance movement producing greater removal at stronger attraction. When insects are already being consistently directed towards the trap crop, additional long movements provide less benefit and can instead increase the chance of moving beyond the trapping region or crossing field boundaries. Trap-crop allocation also influenced this transition, particularly when only a small proportion of the field was assigned to the trap crop, although attraction strength became the dominant factor once the trap-crop strip was sufficiently large.

This interaction between movement behaviour, attraction and trap-crop allocation is consistent with the broader understanding that trap-crop effectiveness depends on both behavioural responses to host-associated cues and the spatial opportunity for interception. Attraction may arise through plant volatiles, aggregation pheromones or differences in host preference that orient pests towards trap plants (Landolt et al. 1999; Martel et al. 2005; Brzozowski et al. 2020), while crop borders, host connectivity and local movement behaviour can alter whether attracted insects actually reach and remain within the trap crop (Gui et al. 2012; Boiteau et al. 2014). The same level of attraction may therefore lead to different management outcomes depending on whether pest movement is dominated by frequent short steps or includes occasional long displacements. These findings reinforce the distinction between encounter and post-encounter processes established in the underlying trap-cropping

framework. Movement and attraction influence whether pests reach the trap crop, whereas arrestment, retention and removal determine what happens after arrival (Holden et al. 2012; Badenes-Pérez 2025; Holden 2026a; Ahmed et al. 2026b). Importantly, the effect of long-distance movement was context dependent: it enhanced removal when attraction was weak but became disadvantageous as attraction strengthened. This reversal persisted even when short- and long-distance movement were objectively related, showing that an objective relationship between movement processes does not remove their ecological consequences. Accounting for the form of pest movement, rather than only its average spatial scale, may therefore improve predictions of when trap crops are likely to intercept pests effectively and how their performance changes with attraction strength and trap-crop allocation.

5.3 Movement-dependent capture and the interpretation of pitfall trap counts

Pitfall trapping provides a useful ecological setting in which to examine whether mathematical similarity between movement kernels translates into similar sampling outcomes. Trap counts are widely used to infer activity, relative abundance, spatial distribution and community structure of ground-dwelling arthropods, yet capture depends on more than the number of individuals present (Work et al. 2002; Hohbein and Conway 2018). Individuals must physically encounter the trap, so observed counts reflect the interaction between population density, locomotor behaviour and sampling design. This dependence on movement has long been recognised, with capture influenced by activity level, path tortuosity, habitat conditions, trap size, spacing and spatial arrangement (Luff 1975; Crist and Wiens 1995; Koivula et al. 2003; Larsen and Forsyth 2005; Brown and Matthews 2016; Engel et al. 2017; Ahmed et al. 2023). Against this background, the present results show that the form of the movement kernel can itself be ecologically important. Heavy-tailed movement increases the frequency of long displacements, allowing individuals to explore a larger portion of the sampling domain and increasing opportunities to encounter spatially separated traps. In a confined system, where individuals cannot permanently leave the sampling area, this greater spatial exploration can translate into higher cumulative capture. The implication is not simply that more mobile individuals are caught more often, but that two movement processes with comparable characteristic scales can still generate different encounter rates because their displacement structures differ. This extends previous work showing that trap efficiency can change with movement persistence and mobility, and that movement type interacts with trap geometry and arrangement to determine capture (Ahmed and Petrovskii 2019; Ahmed et al. 2023).

The relationship between the kernels is equally important. Similar trap counts can arise from distinct movement processes under some parameterisations, whereas objectively related thin- and heavy-tailed kernels can remain ecologically distinct. This echoes earlier findings that Brownian- and Lévy-type movement may produce comparable boundary or trap counts over particular parameter ranges, making the underlying movement process difficult to infer from capture data alone (Bearup et al. 2016; Ahmed and Petrovskii 2019; Ahmed et al. 2025). The present study therefore reinforces an important limitation of trap-based monitoring: similarity in capture does not necessarily imply similarity in movement, while differences in capture do not necessarily indicate differences in abundance. This distinction is

especially relevant because pitfall data are often compared across habitats, seasons or taxa in which locomotor activity can vary independently of density. Temperature, vegetation structure, resource availability, sex, life stage and species-specific behaviour can all alter movement and therefore encounter probability (Melbourne 1999; Koivula et al. 2003; Schmidt et al. 2006; Yamashita et al. 2010; Engel et al. 2017). Likewise, sampling geometry can modify how movement differences are expressed. Previous studies have shown that trap shape, spacing and arrangement can alter capture efficiency, sometimes non-linearly, and that the relative performance of sampling designs depends on the spatial scale of movement (Miller et al. 2015; Brown and Matthews 2016; Ahmed and Petrovskii 2019; Ahmed et al. 2023). The comparatively small difference between grid and transect configurations here should therefore be interpreted as context dependent rather than as evidence that arrangement is generally unimportant.

The broader implication is that pitfall counts should be interpreted as movement-dependent observations rather than direct measures of population size. Mechanistic movement models can help separate changes caused by population abundance from those arising through altered movement behaviour or sampling geometry, improving both ecological interpretation and sampling design (Petrovskii et al. 2012, 2014; Miller et al. 2015; Ahmed et al. 2023). In this sense, objectively relating thin- and heavy-tailed kernels provides a useful baseline for identifying when differences in capture reflect genuine consequences of movement structure rather than arbitrary choices in how alternative movement processes are parameterised.

5.4 Movement-dependent planar interception in three-dimensional space

Flying insects provide a particularly clear example of how differences between movement kernels can be translated into ecological outcomes through spatial geometry. Flight occurs in three dimensions, while many monitoring and control devices are finite planar surfaces that must be physically intersected before capture can occur. Recent developments in three-dimensional movement modelling allow directional persistence, attraction and spatial exploration to be represented explicitly (Benhamou 2018; Ahmed et al. 2021b; Klappstein et al. 2026), complementing rapid advances in technologies capable of resolving insect flight trajectories in three dimensions (Kirkeby et al. 2016; Batista et al. 2019; Sun and Gaydecki 2021; Dedic et al. 2024). Such models are particularly relevant for flying animals because reducing movement to two dimensions can obscure ecologically important interactions with vertically structured environments and targets (Ahmed et al. 2021b; Klappstein et al. 2026). Previous three-dimensional trapping models have shown that capture depends on the interaction between movement behaviour and trap geometry rather than on trap size alone. For volumetric traps, capture varies non-linearly with surface area and movement diffusion, while trap shape can also influence efficiency (Ahmed et al. 2021b). More recently, planar interception modelling has distinguished the probability of reaching a trapping surface from retention after contact and from edge leakage, where an insect crosses the plane of the trap outside its finite boundaries (Ahmed et al. 2026a). This distinction is ecologically important because increasing attraction or retention cannot guarantee capture if trajectories fail to intersect the trapping surface in the first place. Empirical studies similarly show that trap-

associated cues can alter flight direction and approach behaviour, while initial contact does not necessarily result in retention (Hawkes and Gibson 2016; Cribellier et al. 2018; Rehling et al. 2025).

The present comparison adds movement-kernel structure to this geometric interpretation. Even when short- and long-distance kernels were objectively related, heavy-tailed movement remained less readily intercepted by the finite panel. Occasional long displacements increase the possibility that an individual crosses the panel plane beyond the trapping surface, creating a geometric route to interception failure through edge leakage. The ecological implication is therefore not simply that long-distance movement changes the rate of spatial exploration, but that its effect depends on the geometry of the target being encountered. This contrasts with the confined pitfall system, where greater spatial exploration generally creates additional opportunities for trap encounter. In three-dimensional planar interception, the same capacity for larger displacement can instead carry individuals beyond the finite target. This mechanism is particularly relevant because insect flight behaviour is highly context dependent. Directional responses can change with visual and olfactory cues, physiological state and environmental conditions (Reynolds and Frye 2007; Osborne et al. 2013; Hawkes and Gibson 2016; Wainwright et al. 2017), while differences among species, sexes and reproductive states may alter flight speed, persistence and spatial extent (Rund et al. 2012; Somerville et al. 2019; Dong et al. 2025). Trap performance may therefore differ among populations exhibiting different movement characteristics even when trap design and abundance are unchanged. Likewise, increasing panel size can reduce opportunities for edge leakage, but trap effectiveness will still depend on how movement interacts with attraction, geometry and retention (Esterhuizen et al. 2011; Sbaraglia et al. 2025; Ahmed et al. 2026a).

For planar monitoring systems, the broader implication is that finite trap geometry can amplify differences that remain between optimally related movement processes. Sticky cards, coloured panels and other interception surfaces should therefore not be interpreted solely in terms of attraction or surface area (Epsky et al. 2008; Benthall et al. 2022; Roberts et al. 2025). Incorporating species- and context-specific movement behaviour into three-dimensional interception models may improve interpretation of trap catches and help distinguish low capture caused by weak attraction, geometric bypass or poor retention. More generally, these results show that objectively relating movement kernels does not remove the ecological consequences of their different displacement structures when movement interacts with spatially constrained targets.

6. Conclusion

Relating short- and long-distance movement kernels provides an objective basis for comparing fundamentally different dispersal processes, but mathematical similarity does not imply ecological equivalence. Our results show that differences retained in the displacement structure of thin- and heavy-tailed movement can be amplified, diminished or even reversed depending on the spatial and behavioural context in which movement occurs. Rare long-distance displacements may increase opportunities for ecological interaction in some settings while reducing them in others, particularly when movement is constrained by boundaries, finite targets or directional responses. The ecological consequences of dispersal therefore

cannot be inferred from the movement kernel alone. They emerge from the interaction between movement behaviour, spatial structure and the processes that follow encounter. Mechanistic models that couple alternative movement kernels with explicit spatial structure can help distinguish ecological consequences arising from genuine differences in movement from those introduced by arbitrary parameterisation. More generally, incorporating movement structure into models of ecological encounters can improve interpretation of observed patterns and strengthen links between individual movement behaviour and emergent ecological outcomes.

Author contribution statement

DA: Conceptualization, Methodology, Software, Formal analysis, Investigation, Validation, Visualization, Funding acquisition, Writing – original draft, Writing – review & editing.

Conflict of interest

The author declares that the research was conducted in the absence of any commercial or financial relationships that could be construed as a potential conflict of interest.

Funding

The author received financial support from Gulf University for Science and Technology, Kuwait. The funder had no role in the study design, data analysis, interpretation of results, manuscript preparation, or decision to submit the article for publication.

Data availability statement

The results presented in this study were generated through numerical simulations. The MATLAB code used to perform the simulations and generate the figures is publicly available on GitHub (https://github.com/daa119/Ecological-consequences-of-movement-kernel-similarity-in-insect-interception-and-trapping).

Acknowledgments

During the preparation of this manuscript, the author used ChatGPT (OpenAI) to assist with the development and refinement of MATLAB simulation code and to improve the language and readability of the manuscript. The author subsequently reviewed and verified the code, reviewed and edited the manuscript, and takes full responsibility for the accuracy and integrity of the study and its findings.

References

Ahmed, D. A., and Petrovskii, S. V. (2019). Analysing the impact of trap shape and movement behaviour of ground-dwelling arthropods on trap efficiency. Methods Ecol. Evol. 10, 1246–1264. https://doi.org/10.1111/2041-210X.13207

Ahmed, D. A., Bailey, J. D., Petrovskii, S. V., and Bonsall, M. B. (2021a). "Mathematical bases for 2D insect trap counts modelling," in Advances in Artificial Intelligence,

Computation, and Data Science, eds. T. D. Pham, H. Yan, M. W. Ashraf, and F. Sjöberg (Cham: Springer International Publishing), 133–159. https://doi.org/10.1007/978-3-030-69951-2_6

Ahmed, D. A., Benhamou, S., Bonsall, M. B., and Petrovskii, S. V. (2021b). Three-dimensional random walk models of individual animal movement and their application to trap counts modelling. J. Theor. Biol. 524, 110728. https://doi.org/10.1016/j.jtbi.2021.110728

Ahmed, D. A., Beidas, A., Petrovskii, S. V., Bailey, J. D., Bonsall, M. B., Hood, A. S. C., et al. (2023). Simulating capture efficiency of pitfall traps based on sampling strategy and the movement of ground-dwelling arthropods. Methods Ecol. Evol. 14, 2827–2843. https://doi.org/10.1111/2041-210X.14174

Ahmed, D. A., Petrovskii, S. V., Bailey, J. D., Bonsall, M. B., and Haubrock, P. J. (2025). Bridging short- and long-distance dispersal in individual animal movement. J. Theor. Biol. 614, 112227. https://doi.org/10.1016/j.jtbi.2025.112227

Ahmed, D. A., Cuthbert, R. N., Fluck, I. E., Hawkes, F. M., and Garrod, G. (2026a). Movement-surface interactions of flying insects in three-dimensional space. EcoEvoRxiv [Preprint]. https://doi.org/10.32942/X2597X

Ahmed, D. A., Tahat, N., Fluck, I. E., Holden, M. H., Bailey, J. D., Badenes-Pérez, F. R., et al. (2026b). Insect movement and spatial dynamics determine trap crop effectiveness. SSRN [Preprint]. https://doi.org/10.2139/ssrn.7122680

Badenes-Pérez, F. R., Shelton, A. M., and Nault, B. A. (2004). Evaluating trap crops for diamondback moth, Plutella xylostella (Lepidoptera: Plutellidae). J. Econ. Entomol. 97, 1365–1372. https://doi.org/10.1093/jee/97.4.1365

Badenes-Pérez, F. R., Nault, B. A., and Shelton, A. M. (2005). Manipulating the attractiveness and suitability of hosts for diamondback moth (Lepidoptera: Plutellidae). J. Econ. Entomol. 98, 836–844. https://doi.org/10.1603/0022-0493-98.3.836

Badenes-Pérez, F. R. (2025). Dead-end trap cropping in pest management. Arthropod Plant Interact. 19, 97. https://doi.org/10.1007/s11829-025-10205-6

Bailey, J. D., Benefer, C. M., Blackshaw, R. P., and Codling, E. A. (2021). Walking behaviour in the ground beetle, Poecilus cupreus: dispersal potential, intermittency and individual variation. Bull. Entomol. Res. 111, 200–209. https://doi.org/10.1017/S0007485320000565

Banks, J. E., and Ekbom, B. (1999). Modelling herbivore movement and colonization: Pest management potential of intercropping and trap cropping. Agric. For. Entomol. 1, 165–170. https://doi.org/10.1046/j.1461-9563.1999.00022.x

Banks, J. E., and Laubmeier, A. (2024). Modeling the effects of trap crop attraction strength, patch dispersion, and biological control on pest suppression. Arthropod Plant Interact. 18, 1151–1159. https://doi.org/10.1007/s11829-024-10106-0

Bartumeus, F., Da Luz, M. G. E., Viswanathan, G. M., and Catalan, J. (2005). Animal search strategies: A quantitative random-walk analysis. Ecology 86, 3078–3087. https://doi.org/10.1890/04-1806

Batista, E. P. A., Mapua, S. A., Ngowo, H., Matowo, N. S., Melo, E. F., Paixão, K. S., et al. (2019). Videographic analysis of flight behaviours of host-seeking Anopheles arabiensis towards BG-Malaria trap. PLoS ONE 14, e0220563. https://doi.org/10.1371/journal.pone.0220563

Bearup, D., Benefer, C. M., Petrovskii, S. V., and Blackshaw, R. P. (2016). Revisiting Brownian motion as a description of animal movement: a comparison to experimental movement data. Methods Ecol. Evol. 7, 1525–1537. https://doi.org/10.1111/2041-210X.12615

Benhamou, S. (2007). How many animals really do the Lévy walk? Ecology 88, 1962–1969. https://doi.org/10.1890/06-1769.1

Benhamou, S. (2018). Mean squared displacement and sinuosity of three-dimensional random search movements. arXiv [Preprint]. https://doi.org/10.48550/arXiv.1801.02435

Benthall, K. J., Avila, N., Leake, L. B., Althoff, E. R., Nielsen, A. L., and Rice, K. B. (2022). Comparison of parasitoid retention on yellow sticky card traps. Fla. Entomol. 105, 167–169. https://doi.org/10.1653/024.105.0210

Berg, H. C. (1993). Random Walks in Biology: New and Expanded Edition. Princeton, NJ: Princeton University Press. https://doi.org/10.2307/j.ctv7r40w6

Boiteau, G., Vincent, C., Leskey, T. C., Colpitts, B. G., MacKinley, P., and Lee, D.-H. (2014). Impact of host plant connectivity, crop border and patch size on adult Colorado potato beetle retention. PLoS ONE 9, e95717. https://doi.org/10.1371/journal.pone.0095717

Bowler, D. E., and Benton, T. G. (2005). Causes and consequences of animal dispersal strategies: relating individual behaviour to spatial dynamics. Biol. Rev. 80, 205–225. https://doi.org/10.1017/S1464793104006645

Brown, G. R., and Matthews, I. M. (2016). A review of extensive variation in the design of pitfall traps and a proposal for a standard pitfall trap design for monitoring ground-active arthropod biodiversity. Ecol. Evol. 6, 3953–3964. https://doi.org/10.1002/ece3.2176

Brzozowski, L. J., Gardner, J., Hoffmann, M. P., Kessler, A., Agrawal, A. A., and Mazourek, M. (2020). Attack and aggregation of a major squash pest: Parsing the role of plant chemistry and beetle pheromones across spatial scales. J. Appl. Ecol. 57, 1442–1451. https://doi.org/10.1111/1365-2664.13689

Bullock, J. M., Kenward, R. E., and Hails, R. S. (2002). Dispersal Ecology. Oxford: Blackwell.

Butail, S., Manoukis, N., Diallo, M., Ribeiro, J. M., Lehmann, T., and Paley, D. A. (2012). Reconstructing the flight kinematics of swarming and mating in wild mosquitoes. J. R. Soc. Interface 9, 2624–2638. https://doi.org/10.1098/rsif.2012.0150

Choules, J. D., and Petrovskii, S. (2017). Which random walk is faster? Methods to compare different step length distributions in individual animal movement. Math. Model. Nat. Phenom. 12, 22–45. https://doi.org/10.1051/mmnp/201712203

Codling, E. A., Plank, M. J., and Benhamou, S. (2008). Random walk models in biology. J. R. Soc. Interface 5, 813–834. https://doi.org/10.1098/rsif.2008.0014

Cook, S. M., Khan, Z. R., and Pickett, J. A. (2007). The use of push-pull strategies in integrated pest management. Annu. Rev. Entomol. 52, 375–400. https://doi.org/10.1146/annurev.ento.52.110405.091407

Cribellier, A., van Erp, J. A., Hiscox, A., Lankheet, M. J., van Leeuwen, J. L., Spitzen, J., et al. (2018). Flight behaviour of malaria mosquitoes around odour-baited traps: Capture and escape dynamics. R. Soc. Open Sci. 5, 180246. https://doi.org/10.1098/rsos.180246

Crist, T. O., and Wiens, J. A. (1995). Individual movements and estimation of population size in darkling beetles (Coleoptera: Tenebrionidae). J. Anim. Ecol. 64, 733–746. https://doi.org/10.2307/5852

Dedic, E., Henry, D., Lihoreau, M., and Aubert, H. (2024). 3D detection of flying insects from a millimeter-wave radar imaging system. Comput. Electron. Agric. 226, 109357. https://doi.org/10.1016/j.compag.2024.109357

Dong, L., Bradford, E. F., Barnett, J. M., and Duvall, L. B. (2025). Post-biting behavioral reprogramming underlies reproductive efficiency in Aedes aegypti mosquitoes. Cell Rep. 44, 116663. https://doi.org/10.1016/j.celrep.2025.116663

Ellis, J., Petrovskaya, N. B., and Petrovskii, S. (2019). Effect of density-dependent individual movement on emerging spatial population distribution: Brownian motion vs Lévy flights. J. Theor. Biol. 464, 159–178. https://doi.org/10.1016/j.jtbi.2018.12.016

Engel, J., Hertzog, L., Tiede, J., Wagg, C., Ebeling, A., Briesen, H., et al. (2017). Pitfall trap sampling bias depends on body mass, temperature, and trap number: Insights from an individual-based model. Ecosphere 8, e01790. https://doi.org/10.1002/ecs2.1790

Epsky, N. D., Morrill, W. L., and Mankin, R. W. (2008). "Traps for capturing insects," in Encyclopedia of Entomology, ed. J. L. Capinera (Dordrecht: Springer), 3887–3901. https://doi.org/10.1007/978-1-4020-6359-6_2523

Esterhuizen, J., Rayaisse, J. B., Tirados, I., Mpiana, S., Solano, P., Vale, G. A., et al. (2011). Improving the cost-effectiveness of visual devices for the control of riverine tsetse flies, the major vectors of human African trypanosomiasis. PLoS Negl. Trop. Dis. 5, e1257. https://doi.org/10.1371/journal.pntd.0001257

Fenoglio, M. S., Videla, M., and Morales, J. M. (2017). Evaluating trap cropping strategies for insect pest control through simulation models. J. Pest Sci. 90, 601–610. https://doi.org/10.1007/s10340-016-0807-y

Gui, L., Boiteau, G., Colpitts, B. G., MacKinley, P., and McCarthy, P. C. (2012). Random movement pattern of fed and unfed adult Colorado potato beetles in bare-ground habitat. Agric. For. Entomol. 14, 59–68. https://doi.org/10.1111/j.1461-9563.2011.00539.x

Hannunen, S. (2005). Modelling the interplay between pest movement and the physical design of trap crop systems. Agric. For. Entomol. 7, 11–20. https://doi.org/10.1111/j.1461-9555.2005.00237.x

Hawkes, F., and Gibson, G. (2016). Seeing is believing: the nocturnal malarial mosquito Anopheles coluzzii responds to visual host-cues when odour indicates a host is nearby. Parasites Vectors 9, 320. https://doi.org/10.1186/s13071-016-1609-z

Hohbein, R. R., and Conway, C. J. (2018). Pitfall traps: A review of methods for estimating arthropod abundance. Wildl. Soc. Bull. 42, 597–606. https://doi.org/10.1002/wsb.928

Hokkanen, H. M. T. (1991). Trap cropping in pest management. Annu. Rev. Entomol. 36, 119–138. https://doi.org/10.1146/annurev.en.36.010191.001003

Holden, M. H., Ellner, S. P., Lee, D.-H., Nyrop, J. P., and Sanderson, J. P. (2012). Designing an effective trap cropping strategy: The effects of attraction, retention and plant spatial distribution. J. Appl. Ecol. 49, 715–722. https://doi.org/10.1111/j.1365-2664.2012.02137.x

Holden, M. H. (2026a). Modeling pest dynamics in trap cropping to improve yield: The effects of attraction, retention, and land allocation. arXiv [Preprint]. https://doi.org/10.48550/arXiv.2606.10605

Holden, M. H. (2026b). Trap cropping to maximize agricultural yield: Balancing land allocation trade-offs between main crop production and effective pest management. Nat. Resour. Model. 39, e70020. https://doi.org/10.1111/nrm.70020

Hooten, M. B., Johnson, D. S., McClintock, B. T., and Morales, J. M. (2017). Animal Movement: Statistical Models for Telemetry Data. Boca Raton, FL: CRC Press. https://doi.org/10.1201/9781315117744

Ings, T. C., and Chittka, L. (2008). Speed-accuracy tradeoffs and false alarms in bee responses to cryptic predators. Curr. Biol. 18, 1520–1524. https://doi.org/10.1016/j.cub.2008.07.074

941 Isaacs, R., Willis, M. A., and Byrne, D. N. (1999). Modulation of whitefly take-off and flight
942 orientation by wind speed and visual cues. Physiol. Entomol. 24, 311–318.
943 https://doi.org/10.1046/j.1365-3032.1999.00144.x
944 James, A., Plank, M. J., and Edwards, A. M. (2011). Assessing Lévy walks as models of
945 animal foraging. J. R. Soc. Interface 8, 1233–1247.
946 https://doi.org/10.1098/rsif.2011.0200
947 Jimenez-Vallejo, D., Gonzalez-Olvera, G., Che-Mendoza, A., Medina-Barreiro, A., Del
948 Castillo-Centeno, F., Crews, S. A., et al. (2026). Drivers of mosquito free-flight and
949 resting behavior indoors. bioRxiv [Preprint].
950 https://doi.org/10.64898/2026.02.11.705377
951 Kareiva, P. M. (1983). Local movement in herbivorous insects: Applying a passive diffusion
952 model to mark-recapture field experiments. Oecologia 57, 322–327.
953 https://doi.org/10.1007/BF00377175
954 Kareiva, P. M., and Shigesada, N. (1983). Analyzing insect movement as a correlated random
955 walk. Oecologia 56, 234–238. https://doi.org/10.1007/BF00379695
956 Kawai, R., and Petrovskii, S. V. (2012). Multiscale properties of random walk models of
957 animal movement: lessons from statistical inference. Proc. R. Soc. A 468, 1428–1451.
958 https://doi.org/10.1098/rspa.2011.0665
959 Kirkeby, C., Wellenreuther, M., and Brydegaard, M. (2016). Observations of movement
960 dynamics of flying insects using high resolution lidar. Sci. Rep. 6, 29083.
961 https://doi.org/10.1038/srep29083
962 Klappstein, N., Michelot, T., Togunov, R., and Mills Flemming, J. (2026). Three-dimensional
963 correlated random walks for animal movement and habitat selection. Ecol. Lett. 29,
964 e70414. https://doi.org/10.1111/ele.70414
965 Koivula, M. J., Kotze, D. J., Hiisivuori, L. K. E., and Rita, H. J. (2003). Pitfall trap
966 efficiency: Do trap size, collecting fluid and vegetation structure matter? Entomol.
967 Fenn. 14, 1–14. https://doi.org/10.33338/ef.84167
968 Kot, M. (2001). Elements of Mathematical Ecology. Cambridge: Cambridge University
969 Press. https://doi.org/10.1017/CBO9780511608520
970 Landolt, P. J., Tumlinson, J. H., and Alborn, D. H. (1999). Attraction of Colorado potato
971 beetle (Coleoptera: Chrysomelidae) to damaged and chemically induced potato plants.
972 Environ. Entomol. 28, 973–978. https://doi.org/10.1093/ee/28.6.973
973 Larsen, T. H., and Forsyth, A. (2005). Trap spacing and transect design for dung beetle
974 biodiversity studies. Biotropica 37, 322–325. https://doi.org/10.1111/j.1744-
975 7429.2005.00042.x
976 Le Roy, C., Bharathi, I., Engels, T., and Muijres, F. T. (2026). Dipteran flight diversity is
977 shaped by aerodynamic constraints, scaling, and evolutionary trade-offs. PLoS Biol.
978 24, e3003473. https://doi.org/10.1371/journal.pbio.3003473
979 Luff, M. L. (1975). Some features influencing the efficiency of pitfall traps. Oecologia 19,
980 345–357. https://doi.org/10.1007/BF00348110
981 Macfadyen, S., and Muller, W. (2013). Edges in agricultural landscapes: Species interactions
982 and movement of natural enemies. PLoS ONE 8, e59659.
983 https://doi.org/10.1371/journal.pone.0059659
984 Martel, J. W., Alford, A. R., and Dickens, J. C. (2005). Synthetic host volatiles increase
985 efficacy of trap cropping for management of Colorado potato beetle, Leptinotarsa
986 decemlineata (Say). Agric. For. Entomol. 7, 79–86. https://doi.org/10.1111/j.1461-
987 9555.2005.00248.x
988 Melbourne, B. A. (1999). Bias in the effect of habitat structure on pitfall traps: An
989 experimental evaluation. Austral Ecol. 24, 228–239. https://doi.org/10.1046/j.1442-
990 9993.1999.00967.x

Miller, J. R., Adams, C. G., Weston, P. A., and Schenker, J. H. (2015). Trapping of Small Organisms Moving Randomly: Principles and Applications to Pest Monitoring and Management. Cham: Springer. https://doi.org/10.1007/978-3-319-12994-5

Nathan, R., Getz, W. M., Revilla, E., Holyoak, M., Kadmon, R., Saltz, D., et al. (2008). A movement ecology paradigm for unifying organismal movement research. Proc. Natl. Acad. Sci. U.S.A. 105, 19052–19059. https://doi.org/10.1073/pnas.0800375105

Osborne, J. L., Smith, A., Clark, S. J., Reynolds, D. R., Barron, M. C., Lim, K. S., et al. (2013). The ontogeny of bumblebee flight trajectories: From naïve explorers to experienced foragers. PLoS ONE 8, e78681. https://doi.org/10.1371/journal.pone.0078681

Petrovskii, S., Bearup, D., Ahmed, D. A., and Blackshaw, R. (2012). Estimating insect population density from trap counts. Ecol. Complex. 10, 69–82. https://doi.org/10.1016/j.ecocom.2011.10.002

Petrovskii, S., Petrovskaya, N., and Bearup, D. (2014). Multiscale approach to pest insect monitoring: Random walks, pattern formation, synchronization, and networks. Phys. Life Rev. 11, 467–525. https://doi.org/10.1016/j.plrev.2014.02.001

Pobozniak, M., Tokarz, K., and Musynov, K. (2020). Evaluation of sticky trap colour for thrips (Thysanoptera) monitoring in pea crops (Pisum sativum L.). J. Plant Dis. Prot. 127, 307–321. https://doi.org/10.1007/s41348-020-00301-5

Rehling, L., Raaz, W., Vaske, J., and Döring, T. (2025). Do we need a scientific standard design for yellow sticky traps? J. Appl. Entomol. 149, 1084–1089. https://doi.org/10.1111/jen.13439

Reynolds, A. M., and Frye, M. A. (2007). Free-flight odor tracking in Drosophila is consistent with an optimal intermittent scale-free search. PLoS ONE 2, e354. https://doi.org/10.1371/journal.pone.0000354

Reynolds, A. M., Leprêtre, L., and Bohan, D. A. (2013). Movement patterns of Tenebrio beetles demonstrate empirically that correlated-random-walks have similitude with a Lévy walk. Sci. Rep. 3, 3158. https://doi.org/10.1038/srep03158

Reynolds, A. M. (2018). Current status and future directions of Lévy walk research. Biol. Open 7, bio030106. https://doi.org/10.1242/bio.030106

Roberts, N. S., Ndayiragije, J. C., Özek, T., Butt, T. M., Karaca, İ., Shah, F., et al. (2025). Visual modelling can optimise sticky trap design for simultaneous monitoring of multiple species of insect pests. Sci. Rep. 15, 17280. https://doi.org/10.1038/s41598-025-01954-8

Rodrigues, L. A. D., Mistro, D. C., Cara, E. R., Petrovskaya, N., and Petrovskii, S. (2015). Patchy invasion of stage-structured alien species with short-distance and long-distance dispersal. Bull. Math. Biol. 77, 1583–1619. https://doi.org/10.1007/s11538-015-0097-1

Rund, S. S. C., Lee, S. J., Bush, B. R., and Duffield, G. E. (2012). Strain- and sex-specific differences in daily flight activity and the circadian clock of Anopheles gambiae mosquitoes. J. Insect Physiol. 58, 1609–1619. https://doi.org/10.1016/j.jinsphys.2012.09.016

Sbaraglia, C., Holm, I. M., Sverdrup-Thygeson, A., Åström, J., and Birkemoe, T. (2025). The shape and material of the flight interception trap matter for beetle sampling. J. Appl. Entomol. 149, 1467–1477. https://doi.org/10.1111/jen.13477

Schmidt, M. H., Clough, Y., Schulz, W., Westphalen, A., and Tscharntke, T. (2006). Capture efficiency and preservation attributes of different fluids in pitfall traps. J. Arachnol. 34, 159–162. https://doi.org/10.1636/t04-95.1

1039 Shelton, A. M., and Badenes-Pérez, F. R. (2006). Concepts and applications of trap cropping
1040 in pest management. Annu. Rev. Entomol. 51, 285–308.
1041 https://doi.org/10.1146/annurev.ento.51.110104.150959
1042 Somerville, A. G. T., Gleave, K., Jones, C. M., and Reimer, L. J. (2019). The consequences
1043 of Brugia malayi infection on the flight and energy resources of Aedes aegypti
1044 mosquitoes. Sci. Rep. 9, 18449. https://doi.org/10.1038/s41598-019-54819-2
1045 Spitzen, J., Spoor, C. W., Grieco, F., ter Braak, C., Beeuwkes, J., van Brugge, S. P., et al.
1046 (2013). A 3D analysis of flight behavior of Anopheles gambiae sensu stricto malaria
1047 mosquitoes in response to human odor and heat. PLoS ONE 8, e62995.
1048 https://doi.org/10.1371/journal.pone.0062995
1049 Sun, C., and Gaydecki, P. (2021). A visual tracking system for honey bee (Hymenoptera:
1050 Apidae) 3D flight trajectory reconstruction and analysis. J. Insect Sci. 21, 17.
1051 https://doi.org/10.1093/jisesa/ieab023
1052 Thomas, C. F. G., Parkinson, L., and Marshall, E. J. P. (1998). Isolating the components of
1053 activity-density for the carabid beetle Pterostichus melanarius in farmland. Oecologia
1054 116, 103–112. https://doi.org/10.1007/s004420050568
1055 Turchin, P. (1998). Quantitative Analysis of Movement: Measuring and Modeling Population
1056 Redistribution in Animals and Plants. Sunderland, MA: Sinauer Associates.
1057 Vaxenburg, R., Siwanowicz, I., Merel, J., Robie, A. A., Morrow, C., Novati, G., et al. (2025).
1058 Whole-body physics simulation of fruit fly locomotion. Nature 643, 1312–1320.
1059 https://doi.org/10.1038/s41586-025-09029-4
1060 Viswanathan, G. M., Afanasyev, V., Buldyrev, S. V., Havlin, S., da Luz, M. G. E., Raposo,
1061 E. P., et al. (2000). Lévy flights in random searches. Physica A 282, 1–12.
1062 https://doi.org/10.1016/S0378-4371(00)00071-6
1063 Wainwright, C. E., Stepanian, P. M., Reynolds, D. R., and Reynolds, A. M. (2017). The
1064 movement of small insects in the convective boundary layer: linking patterns to
1065 processes. Sci. Rep. 7, 5438. https://doi.org/10.1038/s41598-017-04503-0
1066 Wallin, H., and Ekbom, B. S. (1988). Movements of carabid beetles (Coleoptera: Carabidae)
1067 inhabiting cereal fields: A field tracing study. Oecologia 77, 39–43.
1068 https://doi.org/10.1007/BF00380922
1069 Ward, D. F., New, T. R., and Yen, A. L. (2001). Effects of pitfall trap spacing on the
1070 abundance, richness and composition of invertebrate catches. J. Insect Conserv. 5, 47–
1071 53. https://doi.org/10.1023/A:1011317423622
1072 Work, T. T., Buddle, C. M., Korinus, L. M., and Spence, J. R. (2002). Pitfall trap size and
1073 capture of three taxa of litter-dwelling arthropods: implications for biodiversity
1074 studies. Environ. Entomol. 31, 438–448. https://doi.org/10.1603/0046-225X-31.3.438
1075 Yamashita, H., Togashi, K., and Kiritani, K. (2010). Sex-related difference in the ability of
1076 Carabus lewisianus (Coleoptera: Carabidae) to escape from pitfall traps. Can.
1077 Entomol. 142, 589–595. https://doi.org/10.4039/n10-013